CHALMERS

Ice forces on wind turbine structures

KIM ILHO

Supervised by Prof. Lars Bergdahl & Karin Lundgren

Department of Structural Engineering Master Thesis
CHALMERS UNIVERSITY OF TECHNOLOGY
Göteborg, Sweden 2002

Abstract

Results of a FE analysis of interaction between an ice sheet and wind turbine plant are presented and a short review of ice material properties from several literatures is presented.

The purpose of FE analysis is to obtain the ice crushing loads on a vertical offshore wind turbine structure caused by the high ice sheet movement. The main parameters for comparing the results are ice thickness and ice compressive strength. As a result, as ice thickness and ice compressive strength are increased, the total crushing force is increased.

In the another part, a short review is presented of the literature on ice physics, material properties and theoretical ice crushing force formula on vertical and sloping offshore structure. Also several maps of ice condition in the Baltic sea are presented.

CONTENTS

Introduction
Part - I
A Review of ice force in the offshore wind turbine
A.1 Introduction A-1
A.2 Foundation types of the wind turbines in offshore A-1
A.3 Types of ice loading A-1
A.3.1 Static loading A-1
A.3.2 Dynamic loading A-2
A.3.3 Total or global ice load A-2
A.3.4 Local ice load A-2
A.4 Categories of driving forces A-2
A.4.1 Wind drive force A-2
A.4.2 Current drive force A-3
A.4.3 Thermal expansion A-3
A.5 Calculation of ice loads A-4
A.5.1 Static ice loading A-4
A.5.2 Dynamic ice loading A-5
A.6 References A-6
B Background of FE Analysis
B.1 Descriptions B-1
B.1.1 Short background B-1
B.1.2 Finite element method B-1
B.1.3 Purpose B-2
B.1.4 Assumptions of the modeling B-2
B.2 Basic theory of nonlinear material analysis in Diana B-2
B.2.1 Introduction B-2
B.2.2 Elements B-2
B.2.3 Nonlinear material modeling B-3
B.2.4 Incremental-Iterative solution in nonlinear analysis B-4
B.2.5 Euler Stability Analysis B-4
B.2.6 Linear transient analysis B-4
B.3 Modeling of FE analysis B-5
B.3.1 Geometry B-5
B.3.2 Mesh and boundary conditions B-5
B.3.3 Applied material properties B-7
B.4 References B-8
C results of FE analysis modeling
C.1 Ice thickness effects C-1
C.2 Compressive strength effects C-1
C.3 Boundary condition effects C-1
C.4 Buckling effects C-1
C.5 The result of total crushing force C-1
D Conclusions
D.1 Concluding remarks D-1
D.2 Future work D-1
D.2.1 Dynamic phenomenon in the interaction of ice and structure D-1
D.2.2 Strain rate effect of ice compressive strength D-1
D.2.3 Geometry study D-1

Part - II

E Physical properties of ice
E.1 The crystal structure of ice....E-1
E.1.1 Microscopic ice type....E-1
E.1.2 The molecular structure of water....E-1
E.1.3 The ideal atomic structure of the ice crystal (Ih)....E-1
E.1.4 The dislocation movement of ice crystal....E-3
E.1.5 The impurity and ice crystal....E-4
E.2 The characteristics of sea ice....E-4
E.2.1 Types of sea ice....E-4
E.2.2 The structure of sea ice....E-4
E.2.3 The formation of sea ice....E-5
E.2.4 The classification of sea ice structures....E-6
E.3 The density of pure ice....E-7
E.4 Physical and thermal properties of seawater, sea ice and snow....E-8
E.5 References....E-9
F Mechanical properties of ice
F.1 Introduction....F-1
F.1.1 Problems with testing of mechanical properties of ice....F-1
F.1.2 Description of general ice strengths....F-1
F.2 The compressive strength....F-1
F.2.1 Test methods for compressive strength....F-1
F.2.2 Compressive strength of pure ice....F-2
F.2.3 Compressive strength comparison of various ice types....F-2
F.2.4 Compressive strength of sea ice....F-3
F.3 Tensile Strength....F-4
F.3.1 Test methods of tensile strength....F-4
F.3.2 Tensile strength of pure ice....F-4
F.3.3 Tensile strength of sea ice....F-4
F.4 Flexural strength....F-5
F.4.1 Test methods of flexural strength....F-5
F.4.2 Basic description of flexural strength....F-5
F.4.3 Flexural strength of sea ice....F-6
F.5 Shear Strength....F-6
F.5.1 Test methods of shear strength....F-6
F.5.2 Shear strength of sea ice....F-6
F.6 Elastic modulus....F-7
F.6.1 Test methods of elastic modulus....F-7
F.6.2 Basic description of elastic modulus....F-7
F.6.3 Elastic modulus of sea ice....F-8
F.7 Poisson's ratio of sea ice....F-9
F.8 Adhesion strength of sea ice....F-9
F.9 Fracture toughness....F-9
F.10 References....F-10
G ice forces on vertical structures
G.1 Introduction....G-1
G.1.1 Idealized failure mode....G-1
G.1.2 Various failure modes....G-1
G.1.3 Failure for various ice types....G-1
G.2 Crushing failure....G-1

G.2.1 General description of crushing failure G-1
G.2.2 Force exerted due to crushing failure G-2
G.2.3 Theoretical approach G-3
G.2.4 Shear failure G-4
G.3 Buckling failure G-5
G.4 Splitting failure G-5
G.5 Cleavage failure G-5
G.6 Vertical lifting failure G-5
G.7 References G-6
H Ice forces on sloping structures
H.1 Introduction H-1
H.1.1 Advantage in failure comparing to vertical structure H-1
H.1.2 Various failure modes H-1
H.2 Two-dimensional flexural failure H-1
H.2.1 Process of failure H-1
H.2.2 Derivation of two-dimensional analysis formula H-2
H.2.3 Factors affecting the failure modes. H-2
H.2.4 Usage of two-dimensional analysis H-3
H.3 Flexural failure H-3
H.3.1 Empirical relationships H-3
H.3.2 Elastic analysis H-3
H.3.3 Plastic limit analysis H-3
H.4 Crushing failure H-5
H.5 Adfreeze failure H-5
H.6 References H-6
I Schematic map of ice conditions
I.1 Ice condition of the Arctic regions I-1
I.2 Ice condition in the Baltic I-1
I.3 The maps of ice condition in the Baltic I-2
I.4 The ice thickness near Gotland of the Baltic I-2
I.5 References I-4

INTRODUCTION

Recently there are potential needs to build offshore wind turbine structures in the coast of the Baltic sea near Gotland island. When building the offshore wind turbine foundation of these areas, the high load caused by thick ice sheets during winter is one of the critical challenges. Indeed since ice is an extraordinary material and its behaviour, it has led to great difficulties in quantifying the critical loads which exert on the offshore wind turbine structure. The main purpose of this thesis is to develop a model for calculating the ice load during it's interaction with a circular wind turbine structure.

This thesis is divided into two parts; ice force calculation using finite element method (F.E.M) program, *DIANA* , and studies of ice mechanical properties in literatures. In Part - Ⅰ the typical ice force analysis using the FEM program is introduced and in Part - Ⅱ the summary of ice properties, ice failure modes on vertical and sloping structure, and ice condition in the Baltic sea are summarized.

When the analysis of ice force is carried out using the FEM program, there are normally two different approaches; the plastic analysis (*Ralston, Riska, Pukkinen 1983a*) and the creep analysis (*Sinha, 1981, Ponter, Pulkkinen 1985a*). In the plastic analysis the brittle or fracture behaviour of ice is expressed by using the different kinds of yield criteria, and in the creep analysis the time-dependant effect of ice strength is considered. In this thesis the plastic approach based on fracture theory was used basically, and transient dynamic method is added.

PART - Ⅰ

A REVIEW OF ICE LOADS ON THE WIND TURBINES

A.1 Introduction

When designing foundations for offshore wind turbines, the combined action of the overturning moment and the shear forces at the seabed should be considered. Especially the question of the likelihood of experiencing simultaneous occurrences of maximal overturning moment and maximal base shear deserves attention. The forces of the moment and shear are caused by winds, currents, waves and ice in the level of seawater. In cold regions, the critical force against the wind turbine structures would be high force caused by thick ice and the thick ice sometimes induces the pile-up that is the ice action resulting in the dramatic damage to offshore cantilever structure system. Hence it is very important to understand the ice action against structures for solving the related problems with drive forces.

A.2 Foundation types of offshore wind turbines

The structure of wind turbine in offshore can be classified as three types according to type of foundation.

- Gravity-base structures: This structure resists lateral loads solely by its large mass and the friction of shear developed at its base. Various configurations have been suggested. Conical designs reduce the water line area as much as possible in order to minimize ice loads, while providing a wide base for stability. In areas of moderate ice, the upper portion of the structure can be made cylindrical to simplify construction procedures. Full-profile conical and cylindrical structures have been proposed where greater mass is required to resist the impact of large ice features or to provide better stability during construction and tow-out.

- Piled-base structures: This structure develops shear resistance through the use of piles and commonly takes jacket or monopod forms.

- Mixed-base structures: This structure, advisable where soil conditions are unfavorable, resist ice loads by a combination of the shear resistance of a large base and the lateral resistance of short piles.

A.3 Types of ice loading

To calculate the ice failure load, it is convenient to divide ice-loading scenarios into two broad categories (static and dynamic loading).

A.3.1 Static loading

The loading state is static if ice exists in stationary contact with a wind turbine structure and then experiences an increasing load applied to it by natural driving forces. Land fast ice conditions, in which a structure is typically surrounded by more or less uniform ice. The load in this condition may be generated by a combination of wind and current. Wind and current then may act on a large expanse of ice cover and load it slowly against the wind turbine structure, which acts as a single isolated pinning point resisting the applied

driving force. The contact between ice and the wind turbine structure may or may not be initially perfect.

A.3.2 Dynamic loading

The loading state is dynamic if an ice feature is not initially in contact with a wind turbine structure, but arrives to it with appreciable velocity. The loading state differs significantly from static loading in two respects: firstly, the initial contact conditions are invariably irregular and non-uniform; secondly, the duration of the impact is generally determined by the kinetic energy of the moving or impact ice feature, which may come to rest during the moving or impact process.

A.3.3 Total or global ice load

The total or global load sustained by a wind turbine structure is important for considerations of foundation sliding resistance, foundation shear bearing capacity and overturning moment at the seabed of a wind turbine structure. The ice contact areas normally involved for such load considerations are in the range 100-1000 m^2.

A.3.4 Local ice load

The local ice load is used in determining the design and spacing of internal structure members and the dimensions of internal cell units from the stresses value over smaller areas than total ice load area.

A.4 Categories of driving forces

The driving motion of floating ice is caused by three primary driving forces: wind, current and thermal expansion (*Fig A.1*).

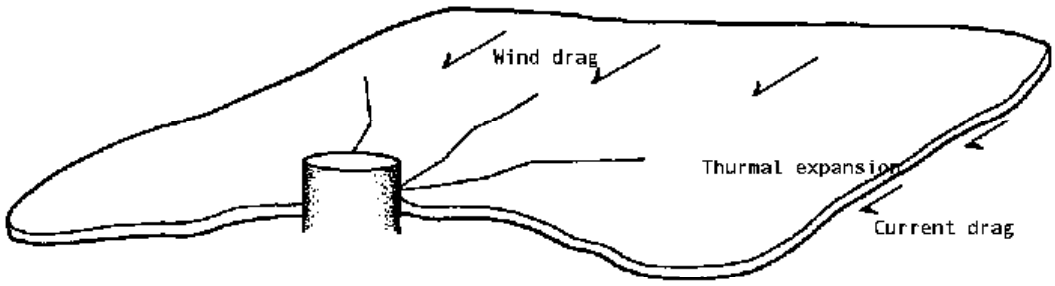

Fig A.1 Principal category of the driving forces for ice action

A.4.1 Wind driving force

Ice driving force by wind develops from drag applied by flow over the rough top surfaces of the ice cover. The general expression of shear force (τ_{wind}) on the ice top surface due to wind is

$$\tau_{wind} = \rho_{air} C_1 \upsilon_1^2 \qquad \text{(A-1)}$$

where ρ_{air} is the density of air which is approximately 1.3 $kg\ m^{-3}$ at low temperature, υ_1 is the velocity (m/s) of wind at special height and C_1 is the drag coefficient for air to depend on the ice type and surface roughness. Generally the wind velocity and drag coefficient is taken at a height of 10 m above the ice surface. Values for C_1 found in

Arctic regions range between 1.0 x 10^{-2} and 3.1 x 10^{-3} (*Banke* and *Smith, 1973*). The drive force (F_{wind}) due to wind drag on an area (A) of ice field is given by

$$F_{wind} = \left(2.5 \times 10^{-3}\right) A \, \upsilon_1^2 \qquad \text{(A-2)}$$

From the Finish Regulations for Structure Loads (*Rakenteiden kuormitusmääräykset*), the driving force (F_{wind}) and the shear forces(τ_{wind})on the ice by wind is

$$F_{wind} = A \, \mu \, \tau_{wind}$$

$$\tau_{wind} = \upsilon_1^2 / 1600 \ (kPa) \qquad \text{(A-3)}$$

where A = the area of the ice floe (m^2), μ = friction factor (0.0010 for smooth ice, 0.0015 for snowy ice, 0.0020-0.0050 for rough and pack ice).

A.4.2 Current driving force

Shear force on the rough bottom surface of ice by current obeys the same law as driving force by wind drag.

$$\tau_{current} = \rho_{water} C_2 \upsilon_2^2 \qquad \text{(A-4)}$$

where ρ_{water} is the density of sea water, υ_2 is the velocity of current at proper depth and C_2 is the drag coefficient for current. The current velocity and drag coefficient is taken at a depth of 1 m below the ice bottom surface. A series of measurements of C_2 have yielded values in the range 2.2 – 8.3 x 10^{-3} for multi-year ice and of about 1.0 x 10^{-3} for first-year ice *(Langleben, 1980*). For general purposes it is reasonable to take a value of 4.0 x 10^{-3}. The drive force ($F_{current}$) due to current drag on an area (A) of ice field is given by

$$F_{current} = 4.1 \, A \, \upsilon_2^2 \qquad \text{(A-5)}$$

A.4.3 Thermal expansion

Thermal driving forces occur when ice undergoes a temperature change and tries to expand. This thermal expansion occurs according to three principal processes.

Surface air temperature changes

Any change of temperature at the surface will propagate slowly downwards through the ice cover, following the Fourier theory of heat conduction. The presence of thermal boundary layers of air makes the efficiency of this process dependent on wind speed. Propagation also depends on the thermal diffusivity of the ice and may be impeded by a surface layer of insulating snow.

Transport

If the ice is permeable as snow, percolation of air, melt water may cause rapid temperature changes. This is unusual, especially for sea ice.

Radiation

Short-wave and long-wave radiation may play important roles in temperature change. Incoming solar radiation and long wave radiation from the atmosphere result in temperature rise, and long-wave radiation emitted back by the ice may result in temperature decrease, especially at night in clear weather. The radiation is strongly dependent on weather conditions, snow cover and absorption characteristics of the ice. Temperature changes are effectively instantaneous at ice surface and lag with depth.

A.5 Calculation of ice loads

Approaches for calculating the ice loads are divided into static and dynamic loadings.

A.5.1 Static ice loading

For a case that the ice is initially adfrozen to the structure and the interaction between ice sheet and structure is perfect, schematic diagram of load history is shown in *fig A.2*. When the driving force, such as wind, which causes the ice sheet to move forward into the structure, is steadily increasing at loading velocity, the interaction typically experiences the separate three stages.

Pure creep

In a continuum mode of pure creep, the ice load is calculated as a function of the ice velocity following the different contact conditions, perfect and imperfect contact.

Transition to fracture

At a certain limiting velocity the ice undergoes a transition between creep behavior and fracture behavior. During this step, the load is near its maximum and velocity may subsequently increase without a corresponding increase in load.

Non-simultaneous fracture

In this step, ice sheet fails in a brittle action and gives rise to a highly variable load history. Generally, the load of this step is lower than those of transition step to fracture. Certainly, a load arising from non-simultaneous fracture is most unlikely to exceed the peak for perfect contact conditions. However, if a sufficiently long period of fracture interaction is experienced then subsequent non-simultaneous failure peaks may exceed the stress at the transition point for irregular contact.

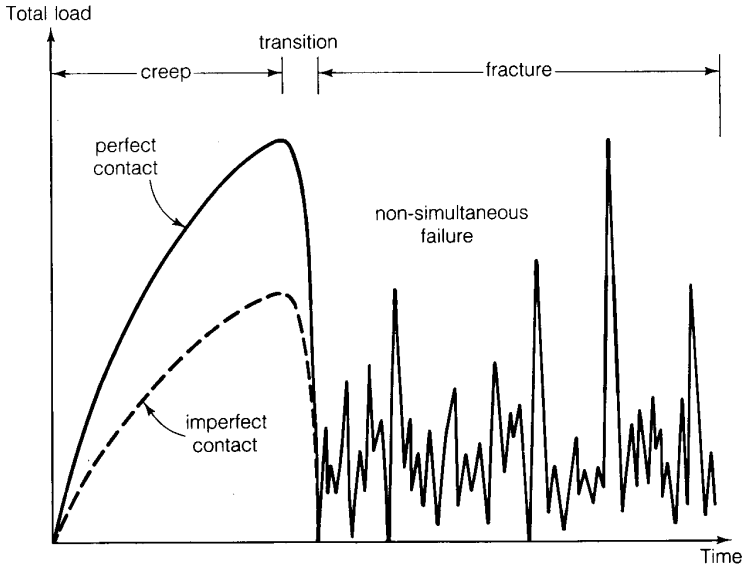

Fig A.2 Schematic diagram of load history during a static ice force

Maximum static force

A typical expression for the maximum static ice force acting on a vertical pile is shown by equation *G.3* to *G.6* of the chapter *G.*

From the Finish Regulations for Structure Loads (*Rakenteiden kuormitusmääräykset*), the maximum static force (P_{static}) due to ice crushing against a vertical structure is

$$P_{static} = k_1 \; k_2 \; k_3 \; b \; h \; \sigma_{ip} \tag{A-6}$$

where k_1 = shape factor for the structure (0.9 for round shape, 1.0 for rectangular shape), k_2 = ice to structure contact factor (1.0 when an adfrozen floe starts moving, 1.5 when a thick ice collar has adfrozen to the structure, 0.5 when ice is cracking continuously), D = width of the structure (at a level 1/3h down from the ice upper surface), h = ice thickness, σ_{ip} = compressive strength of ice (3.0 *MPa* for intact ice moving by the wind or current at the coldest time of winter, 2.5 *MPa* for intact ice moving very slowly e.g. by thermal expansion or shrinking at the coldest time of winter, 1.5 *MPa* for intact ice moving in the spring and the temperature is close to melting point, 1.0 *MPa* for partially weakened melting ice moving at a temperature close to melting point), and k_3 = shape ratio factor

$$k_3 = (1 + 5 \; h / D)^{0.5} \tag{A-7}$$

A.5.2 Dynamic ice loading

In real interaction of moving ice sheet and structure, the load history is near the dynamic phenomena. In dynamic interaction, energy from the moving ice is being transferred and stored as elastic and kinetic energy in the structure. The dynamic response of the structure includes two different forms, transient vibrations with constant amplitudes and frequencies and random vibrations with random amplitudes and frequencies. The latter form is most common in a real situation, but transient vibrations are most dangerous because a resonant condition is always possible. Hence the foundations have to be designed in such a way that there is no chance for a resonant loading, or that the tower itself has vibration isolation to prevent oscillations and high dynamic loads. Normally in case of the transient loading conditions, the maximum stresses and deflections in the structure is twice that in the case of static crushing due to dynamic amplification (*Mauri Määttänen, 1980*).

The main factors affecting the dynamic response with the ice properties such as the static response are the stiffness, mass and damping distributions, ice-induced vibrations of wind turbine structure ranging from 0.5 to 15 *Hz* (if the natural frequencies of structure lie in this range, dynamic interaction is more likely), self-excited vibrations of ice sheets and the shape of natural modes in ice sheets since the amplitude of the natural mode at the ice action point affects the excitation capability of ice force on that particular mode. Indeed among the structure categories or shapes, particularly in the single-pile, cantilever type structures and low aspect ratio structures such as common offshore wind turbine structures, the total dynamic ice force is high.

A.6 References

[1] Erkki Haapanen and Mauri Määttänen, *Offshore Wind Turbine Foundations in Ice Infested Water* .

[2] Mauri Määttänen, Working Group on *Ice Forces on Structures*, PartIII Ice Force on Fixed, Flexible Structures (1980) pp.109-130.

[3] Ken-ichi Hirayama, Joachim Schwarz, and Han-Chin Wu, *An Investigation of Ice Forces on Vertical Structures* (1974).

[4] E.Evgin, C. Zhan, and R.M.W.Frederking, *A Method to Calculate Pack Ice Driving Forces*, Journal of Offshore Mechanics and Arctic Engineering *Volume 6* (1995).

[5] Juri Kajaste-Rudnitski, Pauli Jumppanen and William M. Sackinger, *Ice Loading upon a Cylindrical Offshore Structure* (1985).

[6] Leonid Brevdo and Andrej Il'ichev, *Multi-modal destabilization of a floating ice layer by wind stress*, Cold Regions Science and Technology, *Volume 33* (2001).

[7] Samy Krishnasamy and S. Kulendran, *Combined wind and ice loads from historical extreme wind and ice data*, Atmospheric Research, *Volume 46* (1998).

[8] Claude Daley, *Ice Edge Contact, A Brittle Failure Process Model*, Mechanical Engineering Series No. 100 (1991).

[9] Jukka Tuhkuri, *Experimental Investigations and Computational Fracture Mechanics Modelling of Brittle Ice Fragmentation*, Mechanical Engineering Series No. 120 (1996).

[10] Wang Shuqin, *A Dynamic Model for Breaking Pattern of Level Ice by Conical Structure*, Mechanical Engineering Series No. 156 (2001).

B BACKGROUND OF THE FE ANALYSIS

B.1 Descriptions

B.1.1 Short background

Fig B.1 The assumption of site for modelling

Ice forces acting on the vertical offshore structure (in this theses, wind turbines) is due to relative movements of the structure and ice that are resulted by wind and current (see *Fig B.1*). At first the ice crushes locally and force increase until it is large enough to fail the ice and then the force decreases. The observed basic failure modes of ice can be characterized as crushing with flaking and buckling. These failure modes are a function of velocity of ice movement resulted from wind or current, temperature, thickness of ice, contact width of offshore structure, and inclination of structure (*Timco, 1986; Sanderson, 1988; Sodhi, 1988*) and also depend on ice properties such as ice type (S1 or S2), grain orientation, or loading velocity (from *J.Tuhkuri, 1995*).

B.1.2 Finite element method

Finite element analyses are indispensable in the continuously changing and innovating world of engineering. Demands for a more efficient usage of materials and increasingly more complex structures compel engineers to perform highly accurate analyses. The method used in this work was to make a simple two-layer model for the ice and the

interface between ice and water by using *DIANA*, one of FEM software and to carry out the response analyses.

DIANA

DIANA is a finite element analysis software program and in this work, linear static, transient nonlinear, *Euler* stability analysis, and interface functions were combined.

Methods

There are two common approaches performing the analysis by FEM; a) the plastic analysis (*Ralston, Riska, Pukkinen 1983a*) and b) the creep analysis (*Sinha, 1981, Ponter, Pulkkinen 1985a, Zhan, 1993*). The brittle or fracture behavior of ice is used in the plastic analysis and the time-dependent effect of ice strength is considered in the creep analysis. In this thesis the plastic approach was used basically, and transient dynamic method is added.

B.1.3 Purpose

The aim of the finite element modeling in this thesis was to investigate the influence of the ice failures against the vertical circular offshore structure under the deformation load. The parameter data of modeling, ice thickness and different ice strengths, are used to compare the influence of the ice failure according to them. It is of major interest to compare the load force between results of finite element modeling and already existing experimental data from literature.

B.1.4 Assumptions of the modeling

- Sea ice, in general, is an inhomogeneous, anisotropic, and nonlinear viscoelastic material. General ice-structure interaction problems employ sea-ice models that consider the macroscopic structure of the material and assume homogeneity, continuity, and isotropic behavior. Deviations from these assumptions are handled through the effects of grain size and crystallographic orientation.
- Although the data of the sea ice strength is scattered, sea ice yield strength was modeled as constant values of proper researcher's result. Particularly, for the nonlinear behavior of compressive and tensile strength, they were modeled as an ideal plastic material for compressive behavior and exponential softening material for tensile behavior in the plastic area.
- Although sea ice is displaced and strained in the horizontal plane by wind on the upper surface or by current on the lower surface, the wind effect was neglected in this modeling.
- In choosing the element type, the real ice was assumed to act such as a curved shell element.

B.2 Basic theory of nonlinear material analysis in Diana

B.2.1 Introduction

In this chapter, the basic approaches of Diana used to calculate the ice force is introduced. Most of information is obtained in Manual references from Diana.

B.2.2 Elements

Curved shell elements (Q20SH)

The curved shell element was used for ice material. The shell element is a combination of a plane stress element (plane stress element is characterized by the fact that the stress components perpendicular to the face are zero. This element may only be applied if there

is no bending outside the plane of the structure, like in walls) and a plate bending element. In curved shell element, the thickness must be small in relation to the dimensions in the plane of the element respectively and loads may act in any direction between perpendicular to the surface and in the surface. The Q20SH element is a four-node quadrilateral isoparametric curved shell element.

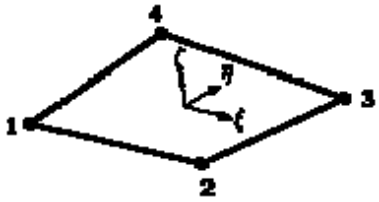

Fig B.2 *Q20H* element

Interface elements (*Q24IF*)
Generally interface elements don't have physical dimensions. They can be used to model specific behaviors in materials such as elastic or nonlinear-elastic embedding and discrete cracking, or to model transitions between parts of a materials such as bond-slip and friction effect between surface elements. In this modeling, interface effects between water and ice are considered. Interface behavior between them is described in terms of a relation between the normal and shear tractions and the normal and shear relative displacements across the interface. The *Q24IF* element is an interface element (plane quadrilateral, 4+4 nodes) between two planes in a three-dimensional configuration.

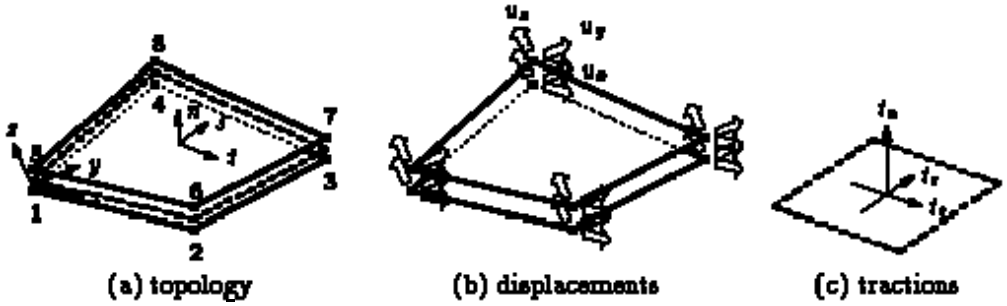

Fig B.3 *Q24IF* element

The basic variables are the nodal displacements (**u**), the relative displacements (**Δu**) and the tractions (**t**).

B.2.3 Nonlinear material modeling

Applicability of nonlinear material properties in Diana
In Diana, there are various methods to consider the nonlinearity of material and geometry such as nonlinear elasticity, plasticity, cracking, viscoelasticity, creep, shrinkage, discrete cracking, bond-slip, friction, and etc. In the ice force modeling, the crack models based on total strain was applied.

The basic concept of the crack models based on total strain combines a cracking model for tension with a plasticity model for compression. Therefore this approach can describe simultaneously the tensile and compressive behavior in one particular element with one stress-strain relationship.

Input data
The input for the crack models based on total strain comprises two parts.

- The basic material properties such as Young's modulus, Poisson's ratio, tensile strength, and compressive strength.
- The definition of the behavior in tension and compression.

B.2.4 Incremental-Iterative solution in nonlinear analysis

In nonlinear analysis, the relation between a force vector and displacement vector is no longer linear but nonlinear. Just as with a linear analysis, we want to calculate a displacement vector that equilibrates the internal and external forces. In the linear case, the solution vector could be calculated right away but in the nonlinear case it cannot. To achieve equilibrium at the end of the increment, we can use an iterative solution algorithm. The combination of both is called an incremental-iterative solution procedure.

- Pure iterative procedure
  Newton-Raphson method, Quasi-Newton method and Constant stiffness method.
- Combination with pure procedures
  Continuation method and the Line Search method.
- Convergence criteria (Process to stop the iteration)
  Force norm, Displacement Norm and Energy Norm

B.2.5 Euler Stability Analysis

Euler stability analysis gives information about `linearized stability' of a structure. It tells whether solutions from linear elastic analysis are stable or whether small disturbances to those solutions exist, requiring no extra external energy. This type of stability analysis does not allow for any physical nonlinearities, geometrical nonlinear effects are only partly taken into account. However, often it is a relatively simple and effective method to get a fair impression of a structure's buckling modes.

- Initial imperfections
- Critical buckling mode
  Generally, the lowest buckling mode is most critical.

B.2.6 Linear transient analysis

The external transient loads are composed of the load sets of the linear static analysis. For transient analyses, time-load diagram must be input in addition to specifying the variation in time of the transient loads. We may apply various types of initial conditions for a linear transient analysis.

- Specification of initial displacements or velocities

B.3 Modeling of FE analysis

B.3.1 Geometry

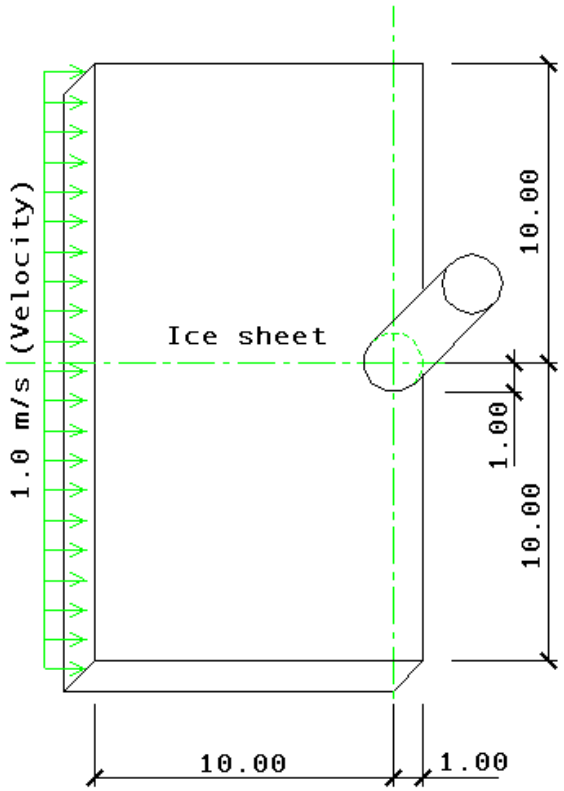

Fig B.4 Geometry of the model

In *Fig B.4* the basic geometry used in this modeling is shown. The ice sheet area is 20 m x 10 *m*, and in the center of one side of this ice sheet, a hole with a diameter 2 m for a vertically cylindrical wind turbine structure is located. The thickness of the ice sheet was varied. The external load of this modeling was expressed as a velocity (1*m/s*), i.e. the total moving velocity of the wind, current, and thermal expansion caused to fail ice sheet against the wind turbine structure. Initial velocity (1*m/s*) of whole sheet was kept constant through the analysis at the edge as shown in *Fig B.4*.

B.3.2 Mesh and boundary conditions

Mesh

Fig B.5 shows the mesh type and mesh arrangement. Meshes were made in two layers, ice sheet for solid material and interface field for stiffening effect of water under loading. In *Fig-B.5*, the mesh with each 833 nodes and each 766 elements for ice and interface elements is shown.

Boundary conditions

The boundary of the ice elements around the hole was fixed in radial direction as shown in *Fig B.6* and the boundary of all interface elements is fixed in *X, Y, Z* direction. To study the boundary condition around holes in *X-Z* direction is complicated since the interface elements are related to the main ice elements. If ice sheet and offshore structure are fully interacted and there is no spring effect between water and ice sheet, the boundary of the ice mesh around the hole would be fixed in *X-Z* direction. On the other hand, if ice sheet and offshore structure do no interact, the boundary of the ice meshes

around hole has same condition such as all ice mesh field. The useful method of friction between ice and structure would be to adjust the tangential stiffness of interface element around hole.

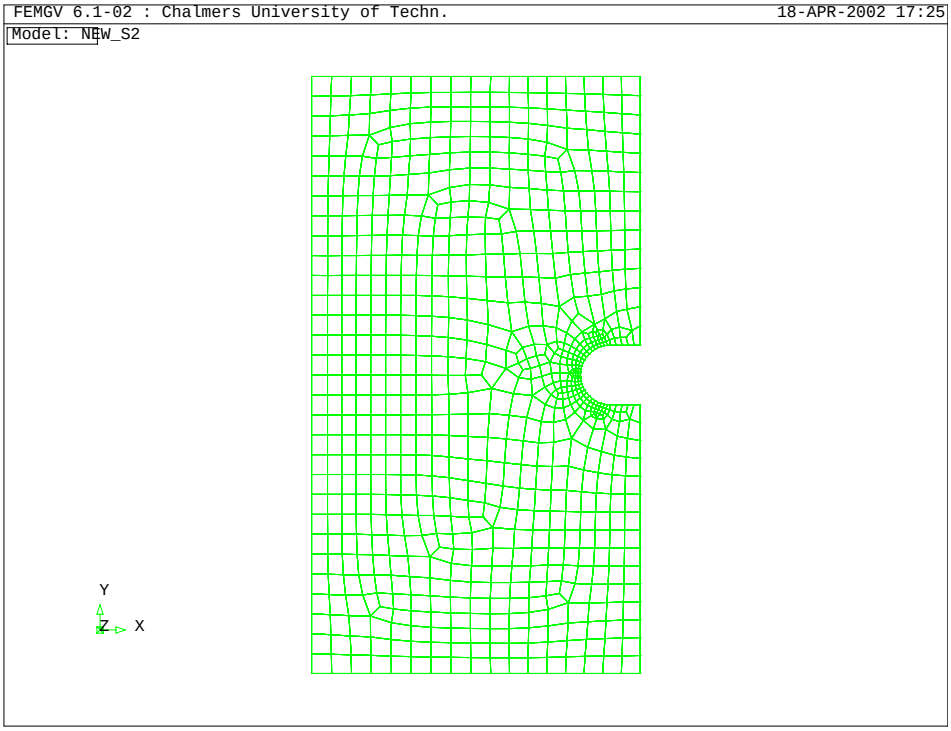

Fig B.5 Mesh and element type of the model

In this thesis, it is assumed that there is no interaction in *X-Z* direction and the tangential stiffness of interface around hole is same as other interface field. But in *X-Y* direction the boundary conditions were fixed. In *Fig B.6,* the boundary conditions around the hole are shown.

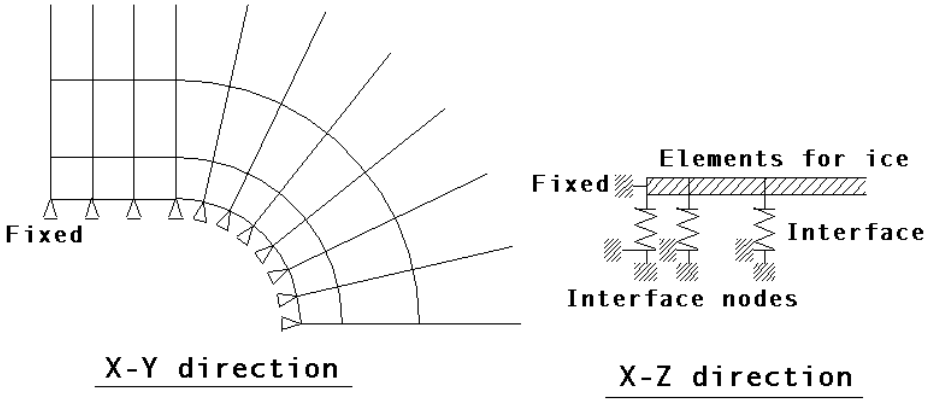

Fig B.6 Boundary conditions

B.3.3 Applied material properties

Ice element

Density (sea ice)	916.8	kg / m^3	Nakawo,1983
Density (sea water)	1028.0	kg / m^3	Dietrich and Kalle,1963
Young's modulus (E)	9.03	GPa	Langleben and Pounder,1963
Poisson's ratio	0.333		Weeks and Assur,1967
Tensile strength	0.4	MPa	Dykins ,1970
Compressive strength	0.7	MPa	Bertil Löfquist,1987
Fracture energy (G_f)	2.328 *1)	J / m^2	Timco and Frederking,1983
Fracture toughness (K_f)	0.145	MN / $m^{3/2}$	Timco and Frederking,1983

*1)Fracture energy (G_f) can be derived from the data for the stress intensity factor (K_f) using the relation $K_f = \sqrt{EG_f}$.

Table B.1 Applied ice material properties

Table B.1 shows the applied material properties of the ice and *Fig B.7* shows the uniaxial stress-strain graph.

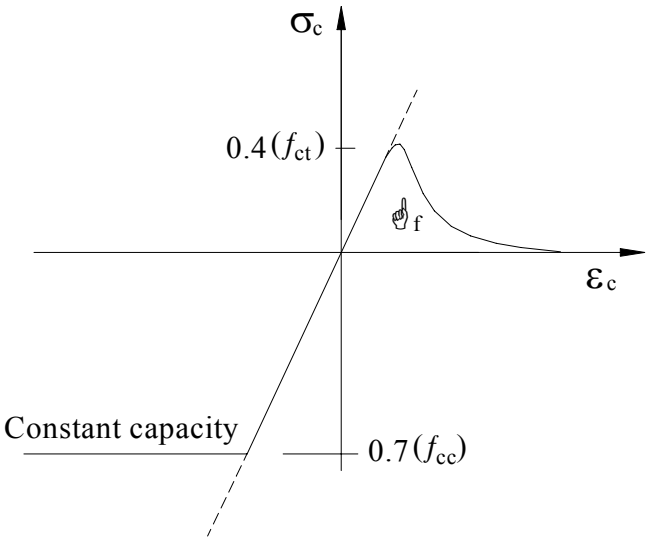

Fig B.7 Assumed stress and strain relationship of the ice

Interface element

The most important material property of the interface is the relationship between traction and relative displacement in the normal direction. The stiffening effect of seawater was considered by applying this relationship. The traction value in tangential direction was very small and the relative displacement was unlimited. *Table B.2* shows the applied interface material properties for the various ice thickness.

Ice thickness	100 mm	200 mm	400 mm
Compression traction (Pa)	108.975	217.950	435.899
Relative displacement (mm)	19.817	21.634	43.268
Tension traction (Pa)	801.277	1602.554	3205.108
Relative displacement (mm)	80.183	178.366	356.732

Table B.2 Applied interface material properties for the normal direction

Fig B.8 shows the relationship of traction and relative displacement of the applied interface elements in normal direction.

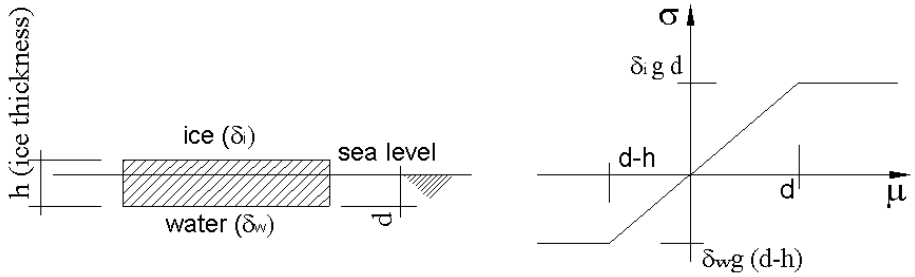

Fig B.8 Traction and displacement relationship of interface element in normal direction (δ_i = density of sea ice, δ_w = density of sea water, u=displacement, σ=traction)

B.4 References

[1] TNO Building and Construction Researcher, *Diana Finite Element Analysis, Users Manual Release 7, Hague, (1998)*.

[2] Juri Kajaste-Rudnitski, Pauli Jumppanen, William M. Sackinger, *Ice Loads upon a Cylindrical Offshore Structure (1985)*

[3] T.D.Ralston, *Plastic Limit Analysis of Sheet Ice Loads on Conical Structure (1979)*, IUTAM Symposium Copenhagen.

[4] E.Pulkkinen, *Comparison between the Creep and the Plastic Analysis of Ice Forces by the FEM (1986)*, Proceedings of the 1st International Conference.

C RESULTS OF FE ANALYSIS MODELING

C.1 Ice thickness effects

In the equations - *G.8, G.9, G.10* of *Part II* the total crushing force (*P*) resulting from the FE analysis increases with the ice thickness (*h*). *Fig C.1* shows the maximum total crushing forces. In the analyses, all initial conditions are the same except for the ice thickness. In equation *G.1* the total crushing forces are increased with the thickness. But the ratio of increased ice maximum crushing forces is not exactly proportional to increased thickness of ice. The increased reaction force seems to be due to buckling effect. It means that the ratio of ice crushing force is high in the thick ice sheet.

The following graphs are results analyzed when the ice compressive strength was 0.7 *MPa*.

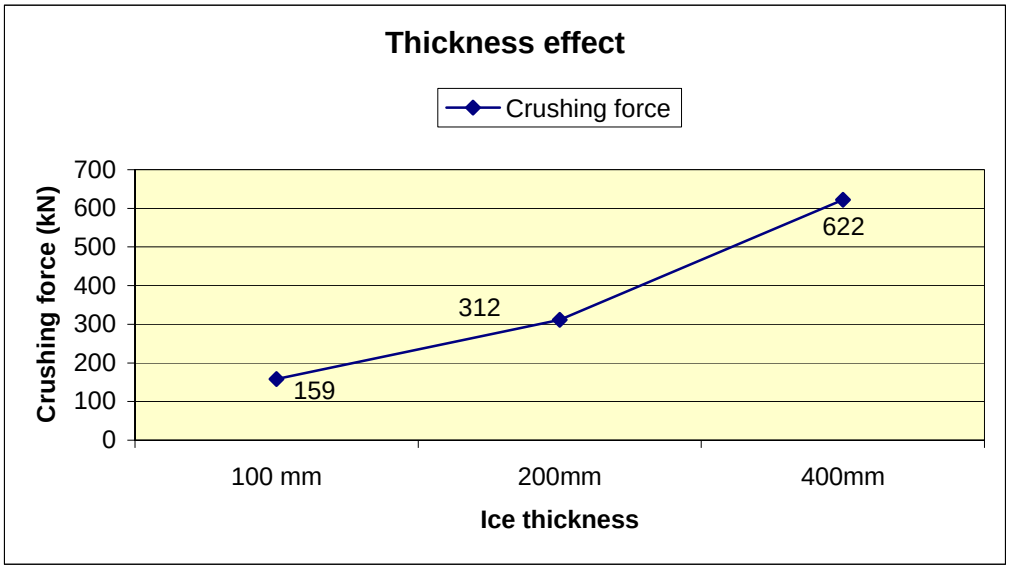

Fig C.1 Total crushing forces for several ice thickness

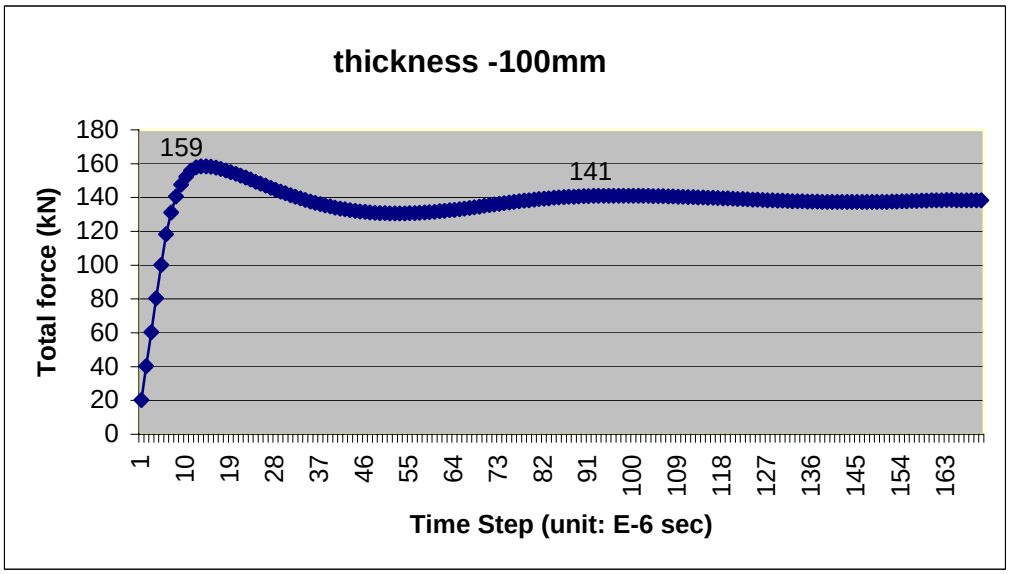

Fig C.2 Reaction force history in *X-X* direction (Ice thickness100mm)

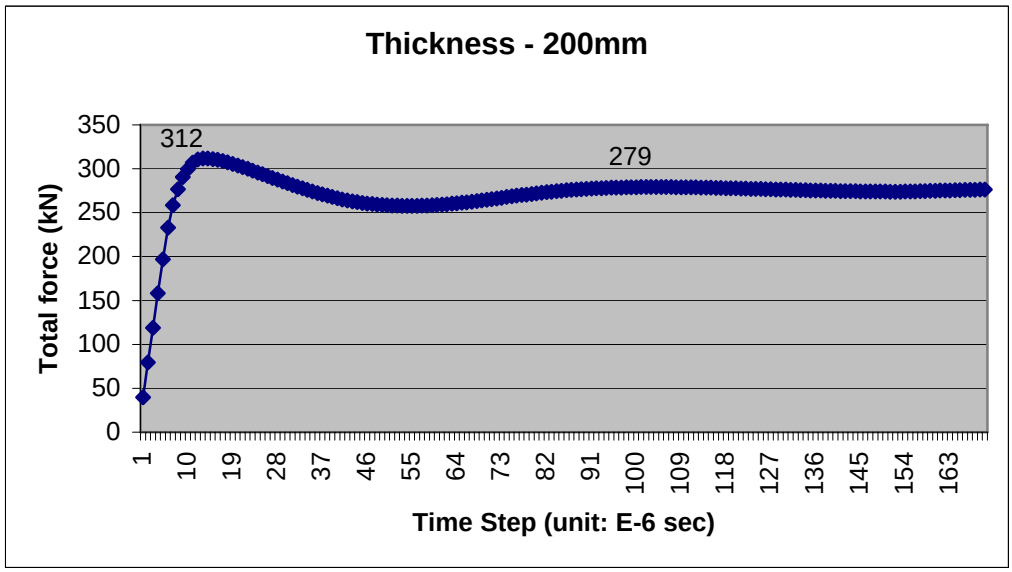

Fig C.3 Reaction force history in X-X direction (Ice thickness 200mm)

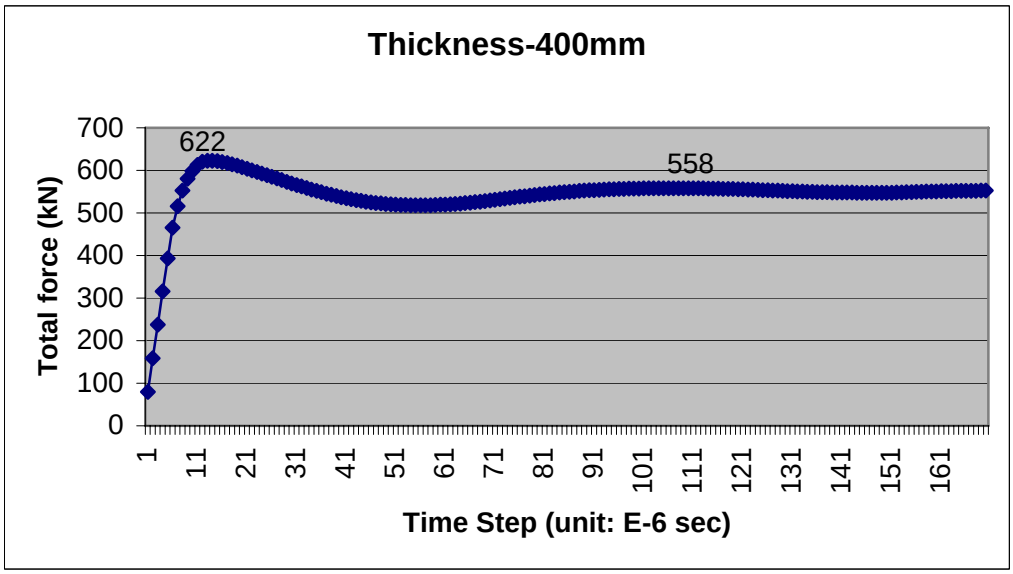

Fig C.4 Reaction force history in *X-X* direction (Ice thickness 400mm)

C.2 Compressive strength effects

Fig C.5 shows results of the first yield crushing force and maximum crushing force for several compressive strengths. When the compressive strength values of ice are 0.7 *MPa* and 2.5 MPa, the first yield crushing force and maximum crushing force are the same. But in case of 5.0 *MPa* and 7.0 *MPa* they are different. As shown in *Fig C.6, Fig C.7*and *Fig C.8,* the analysis has a clear oscillatory response after yielding. Although the total crushing force (*P*) is proportional to the compressive ice strength in the equation *G.8* of *Part Ⅱ*, the results of analysis show that the yield force is not increase unlimitedly but stops around 968kN.

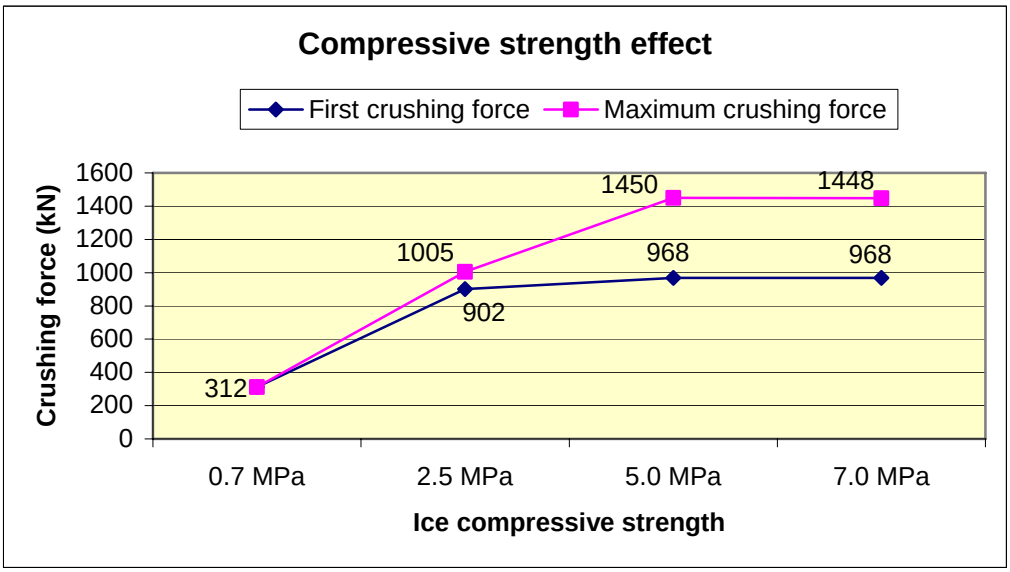

Fig C.5 Two different crushing forces for several ice compressive strengths

In relation to the maximum forces of compressive strength 5.0 *MPa* and 7.0 *MPa*, the vibration after yielding is the self-excited response of the ice. This amplitude of self-excited vibration increases as the compressive strength increases. From the literature (*Mauri Määttänen, 1978*) the ice self-excited amplitudes and frequencies are influenced by the nonlinearity of the ice compressive strength and strain rate. Since the strain-rate of the ice compressive strength was not considered in this analysis, ice self-excited amplitude and frequency are one of various values. Hence for the more idealized dynamic response another approach, the creep analysis, is recommended.

The following graphs are results from analysis when the ice thickness was 200mm.

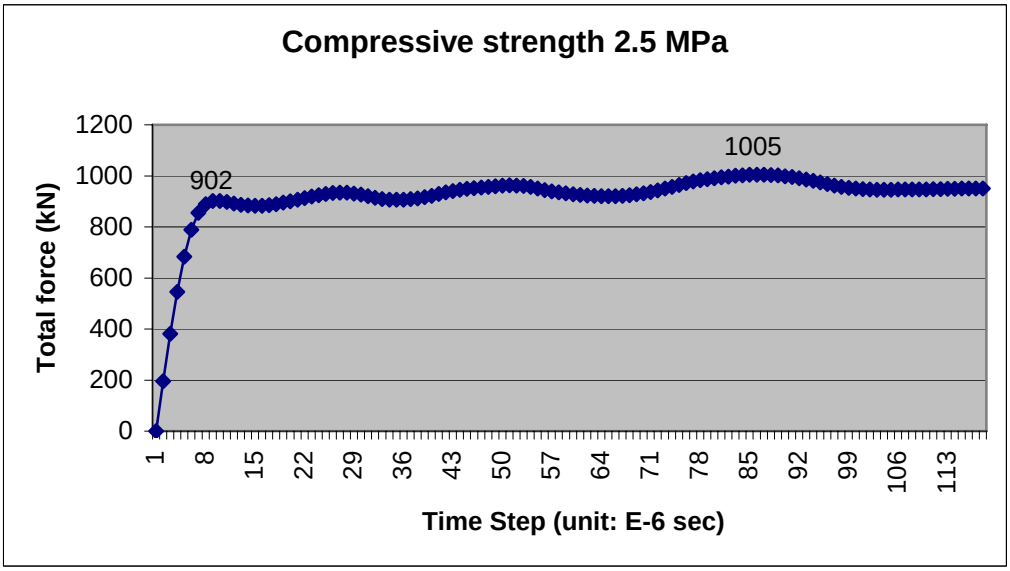

Fig C.6 Reaction force history in X-X direction (Ice compressive strength 2.5 MPa)

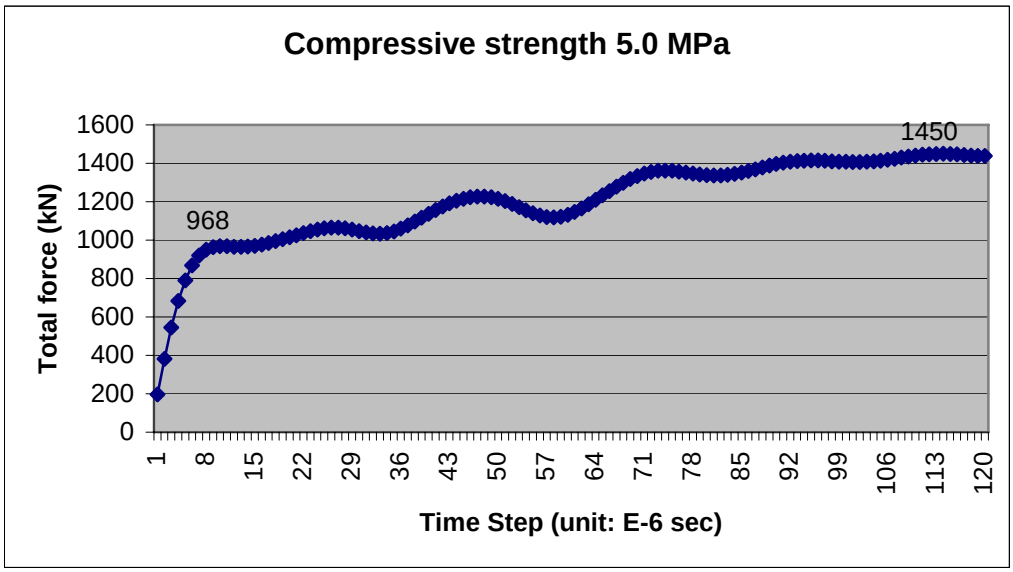

Fig C.7 Reaction force history in *X-X* direction (Ice compressive strength 5.0 MPa)

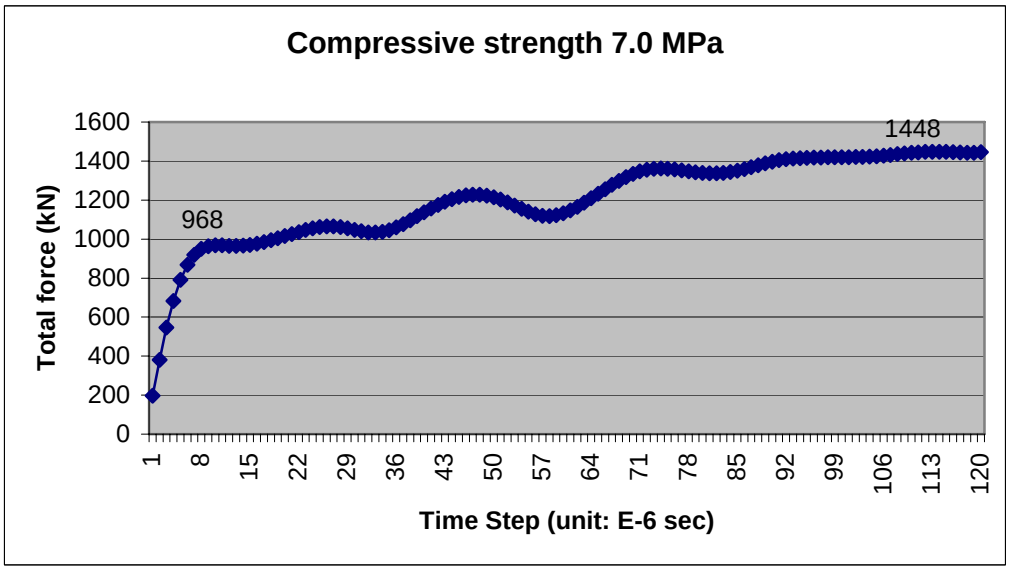

Fig C.8 Reaction force history in *X-X* direction (Ice compressive strength 7.0 MPa)

C.3 Boundary condition effects

Two different boundary conditions around circular hole simulating the offshore structure were studied. In *Fig B.6* the boundary condition of *X-Z* direction was adjusted between the case of free and fixed. However the total reaction force histories were very similar for the two boundary conditions.

C.4 Buckling effects

Buckling failure does not occur for small structure or for thick ice sheets (*Sodhi, and Hamza 1979*, see chapter *G.3* in *Part II*). To determine the buckling effect, the ratio (*D/l*) of structure diameter (*D*) and characteristic ice sheet length (*l*) is the main influencing factor together with the elastic modulus of ice (*E*). In this modeling, the ratio

is 0.2, which is a very low. Therefore, the maximum force will be mainly determined by crushing failure. From literature, the typical buckling process is shown in *Fig C.9*.

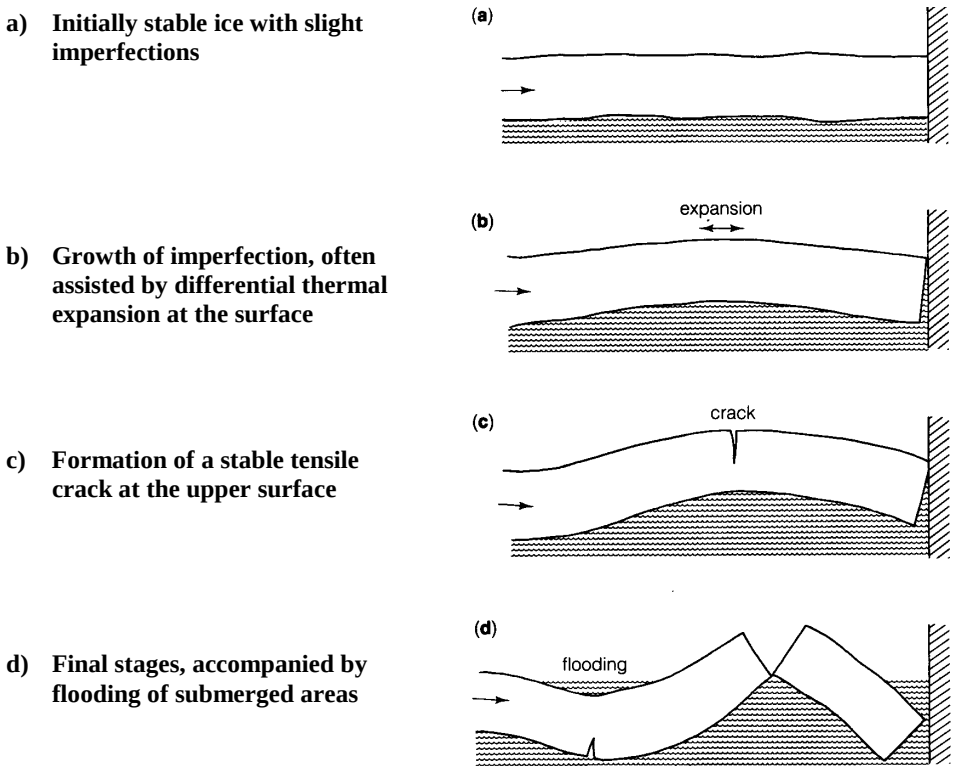

Fig C.9 Four stages of the typical buckling

Although the boundary conditions of the *X-Z* direction around hole have small influence on the total reaction force, it seems to be important for the buckling failure mode. If it is free, there is no buckling effect. But if it is fixed or stiff, the buckling effect can appear. In this modeling the self-weight of ice and imperfection load are initialized for the buckling effect. This result is very similar to *Fig C.9*. Around the fixed boundary and external load position, the buckling effect is started and concentrated.

C.5 The result of the total crushing forces

The following table is the result of total crushing force values in analysed modelling.

Time step (1E-6)	Crushing force (KN)					
	Ice thickness (0.7 MPa)			Ice compressive strength (200 mm)		
	100 mm	200 mm	400 mm	2.5 MPa	5.0 MPa	7.0 MPa
1	20.23	39.79	79.43	196.18	196.18	196.18
2	40.40	79.49	158.68	381.22	381.22	381.22
3	60.47	118.99	237.55	545.71	545.71	545.71
4	80.38	158.21	315.86	683.08	683.08	683.08
5	100.07	197.05	393.43	789.02	790.37	790.37
6	118.25	232.93	465.10	855.46	868.11	868.11
7	131.22	258.39	515.91	888.91	919.47	919.47

8	140.64	276.84	552.74	901.11	949.45	949.45
9	147.72	290.67	580.37	902.04	963.87	963.87
10	152.42	299.83	598.65	897.70	968.35	968.35
11	156.05	306.91	612.82	891.95	967.73	967.73
12	157.93	310.55	620.13	886.96	965.72	965.72
13	158.51	311.66	622.39	883.56	964.79	964.79
14	158.48	311.63	622.40	882.22	966.23	966.23
15	158.20	311.14	621.52	883.00	970.36	970.36
16	157.65	310.17	619.71	885.58	976.85	976.85
17	156.89	308.83	617.17	889.64	985.11	985.11
18	155.99	307.26	614.19	894.68	994.50	994.50
19	155.02	305.58	610.99	900.34	1,004.57	1,004.57
20	153.98	303.78	607.59	906.59	1,015.03	1,015.03
21	152.89	301.90	604.04	913.07	1,025.69	1,025.69
22	151.75	299.93	600.32	918.90	1,036.28	1,036.28
23	150.58	297.91	596.53	924.32	1,046.32	1,046.32
24	149.39	295.86	592.67	929.38	1,055.08	1,055.08
25	148.20	293.79	588.79	933.06	1,061.67	1,061.67
26	147.00	291.71	584.88	934.60	1,065.25	1,065.25
27	145.82	289.64	580.98	933.78	1,065.27	1,065.27
28	144.66	287.58	577.11	930.85	1,061.73	1,061.73
29	143.54	285.53	573.27	926.11	1,055.33	1,055.33
30	142.45	283.51	569.47	920.21	1,047.42	1,047.42
31	141.39	281.54	565.75	914.36	1,039.85	1,039.85
32	140.39	279.60	562.11	909.72	1,034.57	1,034.57
33	139.42	277.72	558.56	906.89	1,033.26	1,033.26
34	138.50	275.90	555.11	905.97	1,036.94	1,036.94
35	137.64	274.14	551.77	906.69	1,045.80	1,045.80
36	136.82	272.45	548.55	908.60	1,059.45	1,059.45
37	136.05	270.83	545.48	911.77	1,076.71	1,076.71
38	135.34	269.30	542.54	916.22	1,096.25	1,096.25
39	134.68	267.85	539.76	922.02	1,116.83	1,116.83
40	134.07	266.49	537.14	928.55	1,137.38	1,137.38
41	133.51	265.22	534.68	935.12	1,156.85	1,156.85
42	133.00	264.05	532.39	940.91	1,174.86	1,174.86
43	132.55	263.00	530.26	945.71	1,191.06	1,191.06
44	132.14	262.06	528.31	948.79	1,204.79	1,204.79
45	131.79	261.22	526.53	951.44	1,215.78	1,215.78
46	131.49	260.47	524.92	954.15	1,223.53	1,223.53
47	131.23	259.83	523.49	956.98	1,227.47	1,227.47
48	131.02	259.28	522.23	959.69	1,227.33	1,227.33
49	130.86	258.82	521.15	961.77	1,222.96	1,222.96
50	130.74	258.46	520.25	962.82	1,214.56	1,214.56
51	130.66	258.18	519.51	962.37	1,202.70	1,202.70
52	130.62	257.98	518.92	960.14	1,188.07	1,188.07
53	130.62	257.86	518.50	956.16	1,171.75	1,171.75
54	130.66	257.81	518.22	950.59	1,155.09	1,155.09
55	130.73	257.83	518.08	944.60	1,139.75	1,139.75
56	130.83	257.91	518.07	939.60	1,127.51	1,127.51
57	130.97	258.06	518.18	935.27	1,119.86	1,119.86
58	131.14	258.26	518.41	931.67	1,117.91	1,117.91
59	131.34	258.53	518.75	928.46	1,122.06	1,122.06

60	131.57	258.85	519.21	925.63	1,132.01	1,132.01
61	131.84	259.22	519.78	922.95	1,146.95	1,146.95
62	132.12	259.66	520.46	921.11	1,165.71	1,165.71
63	132.43	260.15	521.26	920.27	1,186.97	1,186.97
64	132.77	260.69	522.17	919.91	1,209.57	1,209.57
65	133.13	261.27	523.18	920.19	1,232.68	1,232.68
66	133.50	261.89	524.25	921.49	1,255.63	1,255.63
67	133.88	262.55	525.41	924.13	1,277.85	1,277.85
68	134.27	263.25	526.64	927.35	1,298.74	1,298.74
69	134.66	263.98	527.93	931.55	1,317.63	1,317.64
70	135.06	264.74	529.27	936.86	1,333.84	1,333.85
71	135.46	265.51	530.69	943.13	1,346.69	1,346.70
72	135.86	266.28	532.18	949.95	1,355.74	1,355.75
73	136.26	267.05	533.67	957.17	1,360.89	1,360.90
74	136.64	267.81	535.16	964.58	1,362.38	1,362.39
75	137.02	268.56	536.61	971.59	1,360.88	1,360.88
76	137.39	269.29	538.04	977.68	1,357.17	1,357.17
77	137.75	270.00	539.41	983.10	1,352.27	1,352.27
78	138.10	270.70	540.75	987.36	1,347.08	1,347.08
79	138.43	271.40	542.04	991.05	1,342.47	1,342.47
80	138.75	272.07	543.27	994.55	1,339.12	1,339.12
81	139.04	272.72	544.46	997.43	1,337.33	1,337.33
82	139.31	273.34	545.61	1,000.12	1,337.47	1,337.48
83	139.57	273.93	546.71	1,002.43	1,339.74	1,339.74
84	139.80	274.49	547.76	1,004.09	1,344.24	1,344.24
85	140.02	275.01	548.77	1,004.94	1,350.88	1,350.89
86	140.21	275.50	549.73	1,004.78	1,359.21	1,359.21
87	140.39	275.94	550.65	1,003.60	1,368.75	1,368.75
88	140.54	276.35	551.51	1,001.43	1,378.83	1,378.84
89	140.66	276.72	552.31	998.55	1,388.55	1,388.62
90	140.77	277.06	553.06	995.09	1,397.14	1,397.27
91	140.86	277.38	553.74	990.85	1,404.08	1,404.22
92	140.93	277.67	554.35	985.83	1,409.09	1,409.24
93	140.99	277.93	554.90	979.99	1,412.32	1,412.55
94	141.03	278.16	555.39	973.91	1,413.77	1,414.62
95	141.06	278.37	555.82	967.85	1,414.44	1,416.08
96	141.08	278.55	556.22	962.19	1,414.32	1,417.31
97	141.08	278.71	556.56	957.28	1,412.78	1,418.43
98	141.08	278.84	556.86	953.26	1,410.39	1,419.36
99	141.07	278.95	557.11	950.14	1,408.70	1,419.99
100	141.05	279.04	557.35	947.80	1,407.50	1,420.24
101	141.02	279.10	557.56	946.32	1,406.95	1,420.27
102	140.98	279.15	557.74	945.68	1,407.08	1,420.49
103	140.93	279.18	557.89	945.58	1,408.16	1,421.26
104	140.88	279.18	558.01	945.79	1,410.28	1,422.82
105	140.82	279.17	558.09	946.14	1,413.64	1,425.11
106	140.75	279.15	558.14	946.59	1,418.26	1,428.08
107	140.68	279.10	558.16	946.84	1,423.84	1,431.50
108	140.60	279.05	558.14	946.95	1,429.71	1,435.09
109	140.51	278.98	558.09	947.08	1,435.27	1,438.59
110	140.42	278.91	558.01	947.52	1,440.22	1,441.82
111	140.33	278.82	557.89	948.15	1,444.31	1,444.61

112	140.23	278.72	557.76	948.88	1,447.31	1,446.74
113	140.13	278.62	557.59	949.50	1,449.09	1,447.99
114	140.02	278.51	557.39	949.94	1,449.55	1,448.16
115	139.91	278.39	557.17	950.48	1,448.67	1,447.21
116	139.80	278.26	556.93	950.76	1,446.82	1,445.59
117	139.68	278.13	556.66	950.93	1,443.94	1,443.84
118	139.56	277.99	556.37	951.11	1,440.74	1,442.73
119	139.43	277.85	556.06	951.45	1,438.81	1,443.07
120	139.31	277.70	555.72	952.02	1,438.29	1,445.51

Table C.1 Total crushing force values in modeling cases and load steps

The following figures are reaction force history graphs in several nodes.

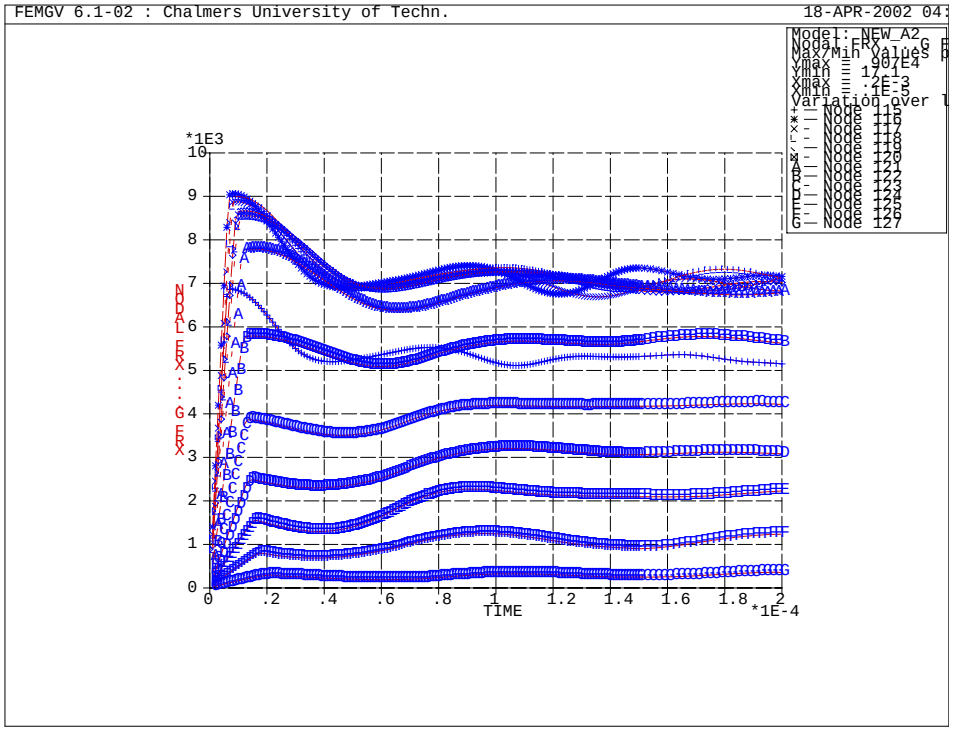

Fig C.10 Reaction force history in several nodes (Ice thickness 100mm)

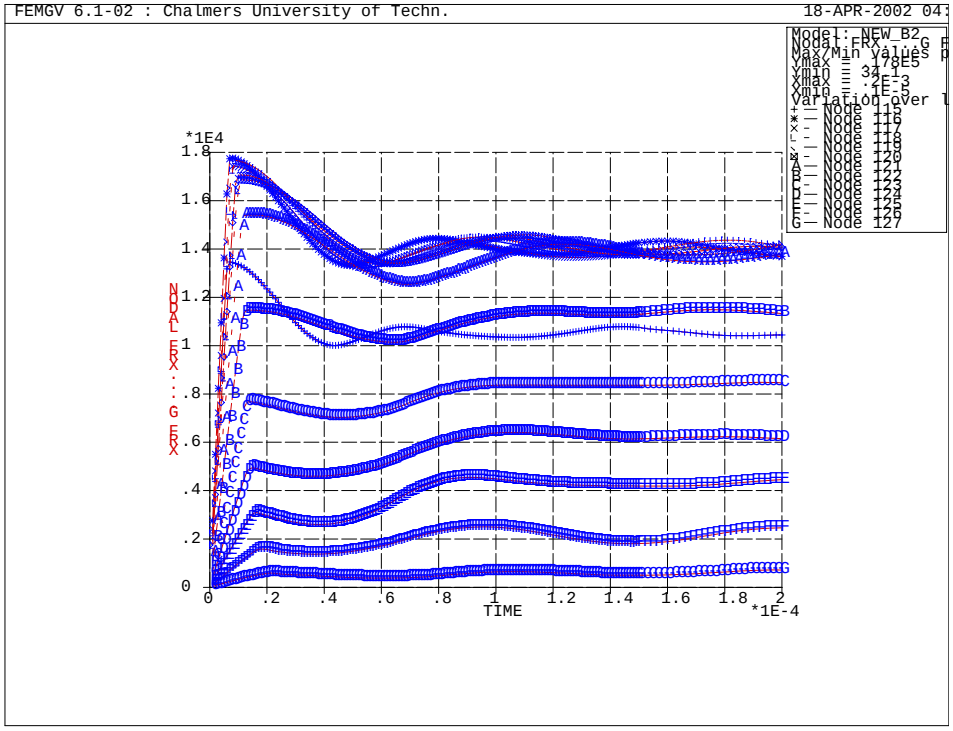

Fig C.11 Reaction force history in several nodes (Ice thickness 200mm)

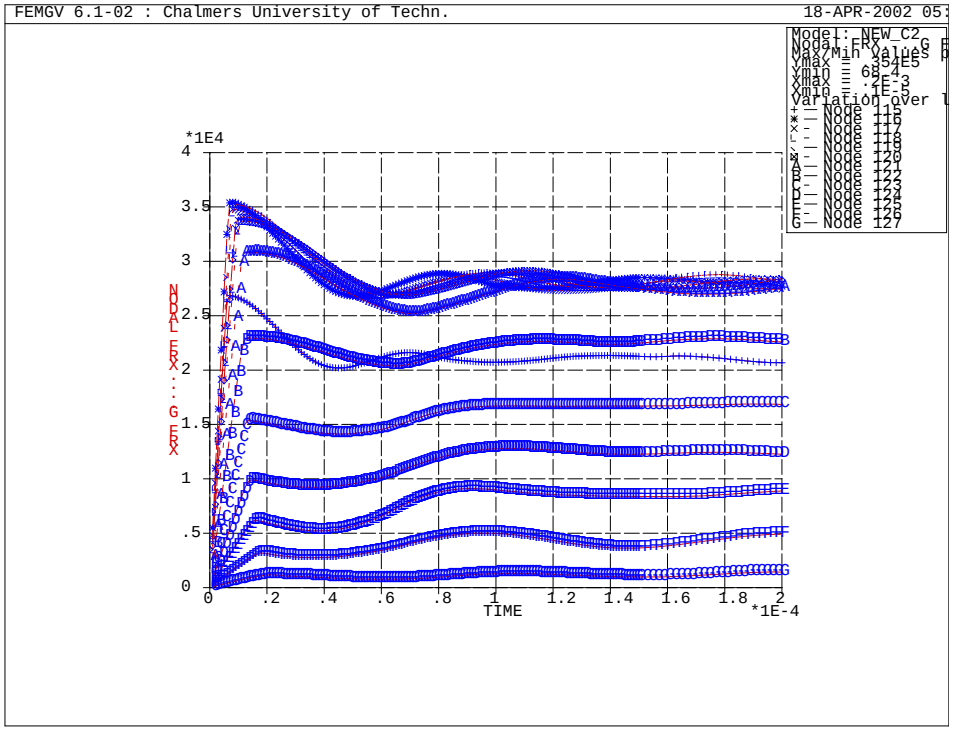

Fig C.12 Reaction force history in several nodes (Ice thickness 400mm)

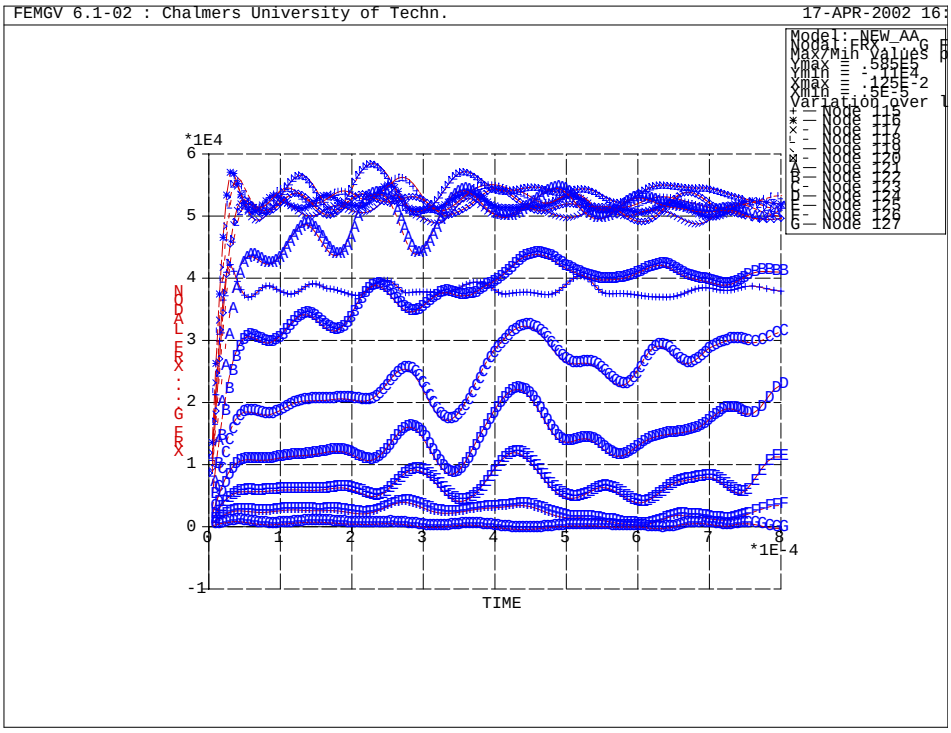

Fig C.13 Reaction force history in several nodes (Ice compressive strength 2.5 MPa)

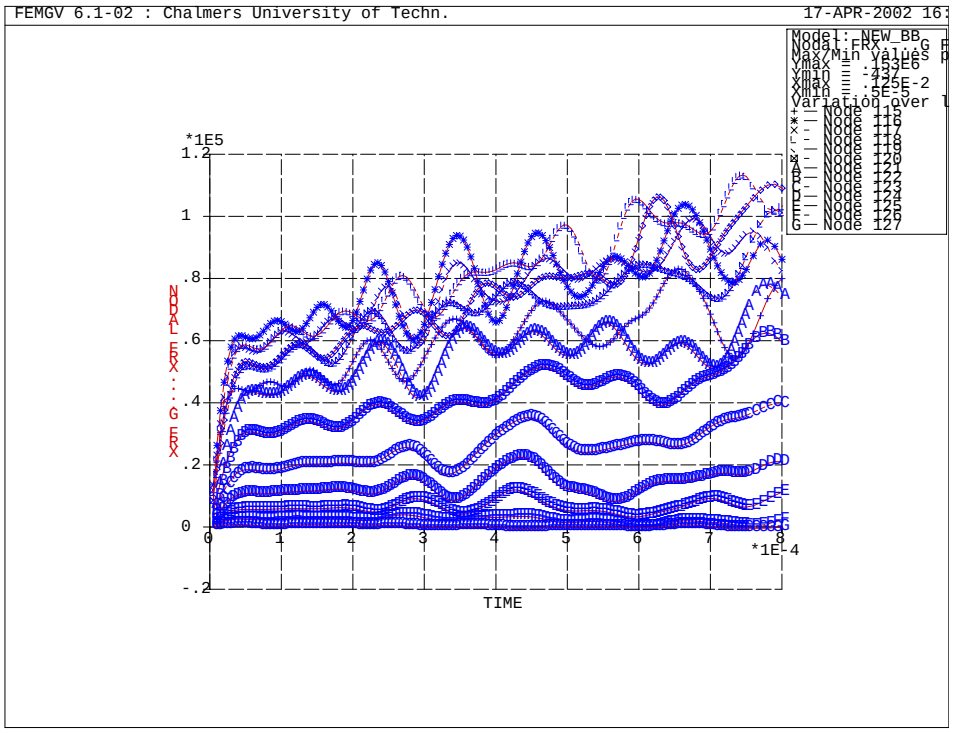

Fig C.14 Reaction force history in several nodes (Ice compressive strength 5.0 MPa)

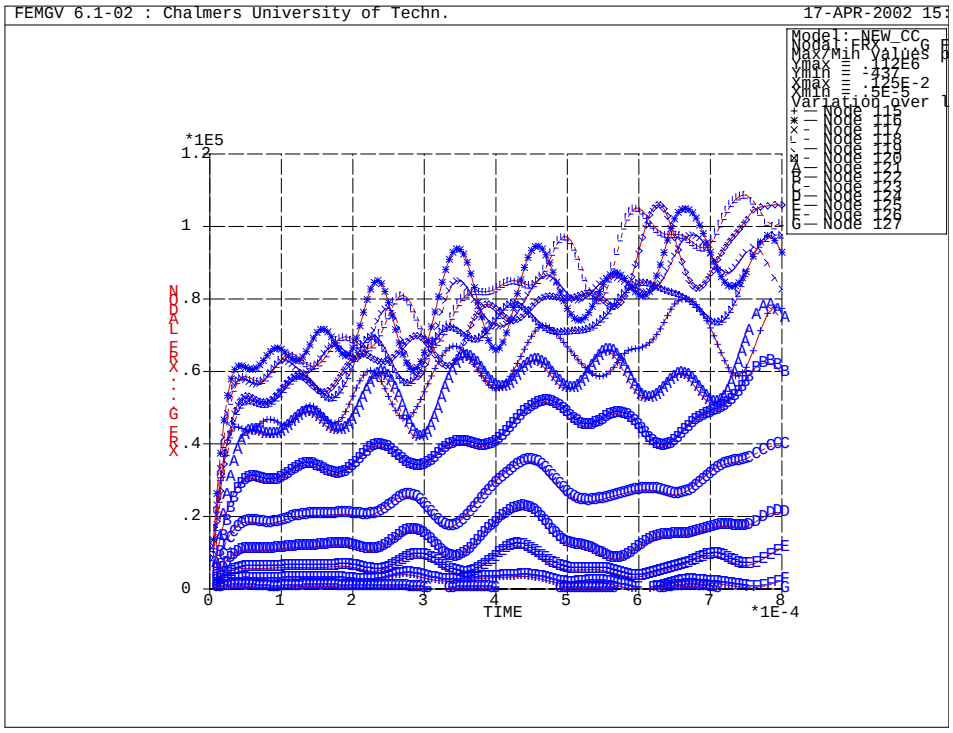

Fig C.15 Reaction force history in several nodes (Ice compressive strength 7.0 MPa)

D CONCLUSIONS

D.1 Concluding remarks

Based on the results of the FE analysis presented in this thesis, the following conclusions were obtained:

- The maximum ice crushing force on vertical structure increases as ice thickness increases although there is a slight buckling effect.
- The ice crushing yield force increases as the ice compressive strength increases until special compressive strength value.
- The amplitude of ice self-excited vibration increases as the ice compressive strength increases.
- The maximum ice crushing force is influenced on slightly by the boundary condition around a circular vertical structure.

D.2 Future work

D.2.1 Dynamic phenomenon in the interaction of ice and structure

The interaction of ice and structure is a dynamic phenomenon. The most commonly observed form of interaction could be characterized as quasi-static. In this thesis, the ice crushes intermittently and causes transient vibrations that decay before the next event of ice crushing as shown in the graphs of the *chapter C* in *Part - I*. But in these graphs the natural frequencies and damping effects of the structure are not taken into account.

D.2.2 Strain rate effect of ice compressive strength

In real ice compressive strength test, the strain rate is one of the most important factors. In the dynamic approach the crushing force of ice depends on the load and time (*Ponter, Pulkkinen 1985a and 1985b, Sanderson*). By combining the plastic analysis of this thesis and time-dependent approach, a better ideal result would be obtained.

D.2.3 Geometry study

When the ice sheet interacts with offshore structure, the total force relating to crushing and buckling failure modes depends on the shape (rectangular or cylindrical) and width of structure. The relationship of these geometries and ice force should be studied variously.

PART - Ⅱ

E PHYSICAL PROPERTIES OF ICE

E.1 The crystal structure of ice

E.1.1 Microscopic ice type

There is only one microscopic type of ice that we can experience. The hexagonal ice (Ih) is the stable form at normal temperatures and pressures. At high pressures (greater than 200 MPa) or low temperatures (below about –110˚C), eight other atomic configurations of ice exist, but they are of concern only under laboratory conditions. Even at the most extreme depths beneath the Antarctic ice cap, which reaches a thickness 4000 m in places, the hydrostatic pressure (35 MPa) is insufficient to allow other forms of ice to be stable.

E.1.2 The molecular structure of water

Ice forms from liquid water and it preserve some of the geometrical features of the water molecule. Liquid water, H_2O, consists of an oxygen atom bonded by electrons to two hydrogen atoms, forming an angle of 104˚ 31’ (*Fig E.1*). The non-linearity of the molecule is due to the presence of two other lone-pair electron orbitals, which form an approximately tetrahedral system with the two bonding orbitals.

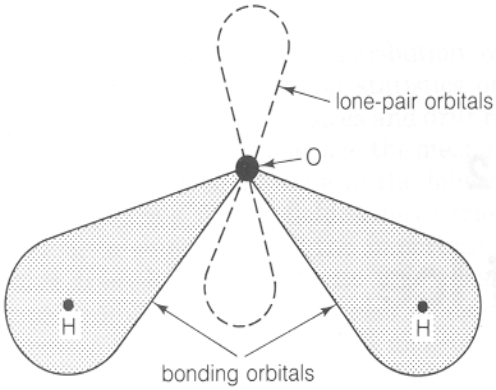

Fig E.1 Molecular structure of a liquid-water molecule

E.1.3 The ideal atomic structure of the ice crystal (Ih)

The atomic structure of the ice crystal (Ih) builds on this tetrahedral geometry of the water molecule: the solid crystal is a repeating tetrahedral coordination of oxygen atoms, in which each oxygen atom is bonded by hydrogen to four other oxygen atoms (*Fig E.2*). Each oxygen atom has two hydrogen atoms closely associated with it, at a distance of about 0.95 *Å* (1 *Å* = 10^{-10} *m*); and two less closely associated with it, at a distance of about 1.76 *Å*. The position of hydrogen atoms on the bonds as shown in *Fig-E.2* is only one possible permutation. There are many other ways of allocating the hydrogen atoms in such a way that each oxygen atom has two hydrogen atoms closely associated with it. The angle between bonds is associated with it. The angle between bonds is about 109˚ 30’, and the individual units of oxygen and hydrogen in ice in fact differ only slightly from the molecular structure of liquid water. The resulting crystal geometry is shown from two other viewpoints in *Fig E.2*. This illustrates that oxygen atoms are well bonded in layers of hexagonal symmetry, but rather less firmly attached from layer to layer: each

oxygen atom has three bonds within a layer but only one bond across to the next layer structure, therefore deformation (gliding and cleavage) preferentially takes place along the layers. The direction perpendicular to the basal plane is referred to as the crystal "c-axis" and is important when describing the various macroscopic crystalline forms of sea ice and glacier ice. *Fig E.2* shows projections of the three dimensional lattice along the most significant crystal directions: looking down the c-axis (*Fig E.2b*), in which the hexagonal plan structure of the basal plane layers is clearly visible; and looking along the layers, perpendicular to the c-axis (*Fig E.2c*), showing the relatively sparse bonding from layer to layer. A single hydrogen atom is associated with each bond.

Fig E.2a)
General view of the crystal structure of ice Ih, showing the tetrahedral constituent unit. (*Michel, 1978*)

Oxygen atoms are shown as black, hydrogen atoms as white. Each bond is associated with a hydrogen atom, and each oxygen atom has two hydrogen atoms particularly closely associated with it. One possible arrangement of hydrogen atoms is schematically illustrated.

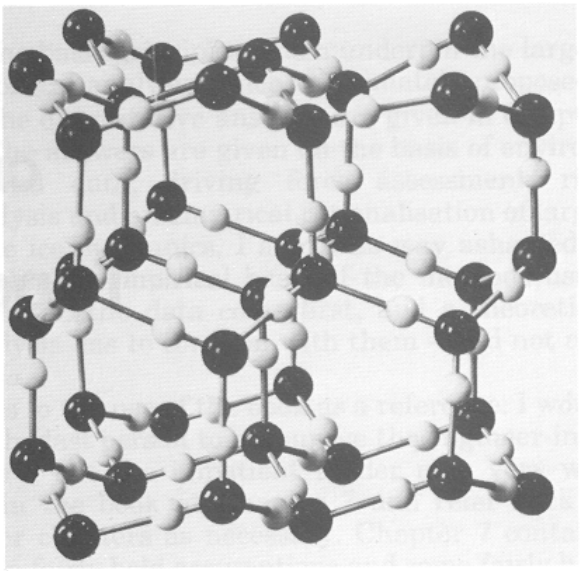

Fig E.2b)
View of crystal lattice looking along the c-axis. The hexagonal structure within a layer is clearly visible.

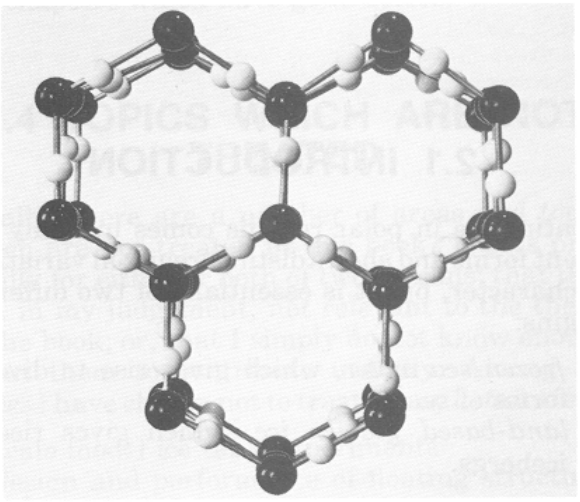

Fig E.2c)
View of crystal lattice looking along basal plane layers, perpendicular to the c-axis

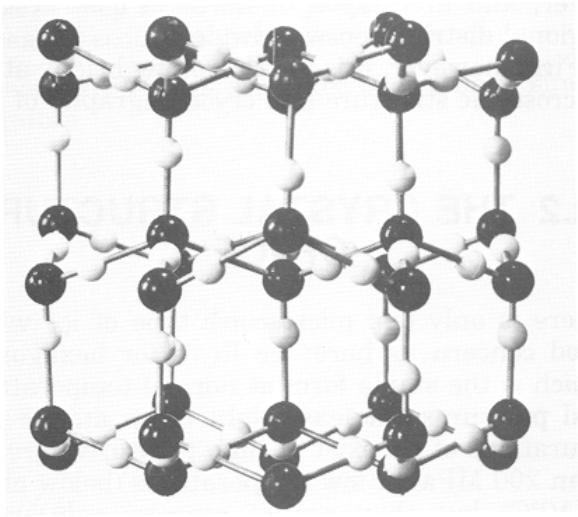

E.1.4 The dislocation movement of ice crystal

An ideal perfect crystal of ice in this form would be extraordinarily difficult to deform permanently, since all possible bonds on the H_2O molecular unit have been made. In practice, however, numerous point defects exist in ice, where a bonding is formed either by two hydrogen atoms or not at all (*Fig E.3a*). This feature allows easy travel of dislocations through the ice crystal by a process of switching of hydrogen atoms between bond-sites, and is responsible for the well-known creeping properties of ice. *Fig E.3b* and *Fig E.3c* illustrate this process: as a defect travels through the crystal, the net effect is a permanent deformation of the crystal.

Fig E.3)
The process of dislocation movement through an ice crystal (*Glen, 1968*)

a) Perfect "ideal" crystal of ice Ih, with one hydrogen atom at each bond site.

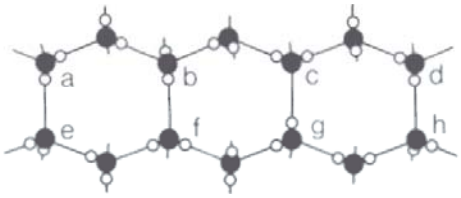

b) Passage of a dislocation system through the crystal, creating defects.

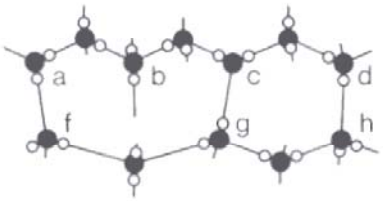

c) Defects of two types, as the dislocation continues moving through the crystal. type-D: with two hydrogen atoms at a bond site (b-g in the figure).
Type-L: with no hydrogen atom at a bond site (c-h in the figure).

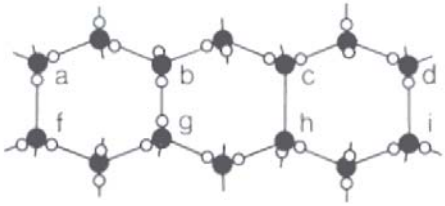

E.1.5 The impurity and ice crystal

Ice crystals are generally of extremely high purity, irrespective of the composition of the water from which they form. This is because very few chemical substances have the correct size and valence to substitute effectively into the ice lattice. There are some possibilities, including some fluoride- and ammonia- based compounds (for instance, F^-, HF, NH_4^+, NH_3, NH_4OH, NH_4F) and some hydro-halogen acids (*Weeks and Mellor, 1984*) but, in general, impurities are very efficiently rejected as the crystal lattice is formed. Impurities seldom account for more than 0.02 mole per cent of the ice crystal. This is an important point to recognize when dealing with sea ice: although formed from a strong saline solution (sea water), the solid ice itself contains a negligible amount of salt. Any gross saltiness of the ice is due only to trapped solution or trapped salt crystals but not to any incorporation of salts into the ice crystal structure. This means that the mechanical properties of sea ice are not substantially different from those of pure ice, provided that appropriate allowance is made for the presence of fluid pockets trapped within the matrix of pure ice.

E.2 The characteristics of sea ice

E.2.1 Types of sea ice

In the offshore marine environment, only two fundamentally different ice types exist - sea ice and glacial ice. Sea ice is formed by the cooling and freezing of seawater, whereas glacial ice originates on land from snow falling on perennial snow fields. This thesis discusses the morphology of the former.

E.2.2 The structure of sea ice

Sea ice typically consists of individual grains of macroscopic dimensions whose orientation can vary. In the process of growth, each grain consists of uniform plates of pure ice, with average thickness of 0.5 to 0.6 *mm*, where the plates are uniformly oriented. Foreign inclusions and brine are partly displaced to the intergranular boundary, but a considerable part of the brine remains in the cells within the grains (*Fig E.4*)

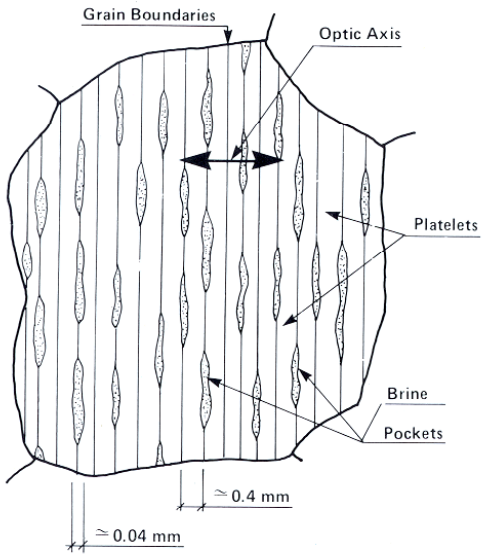

Fig E.4 Macroscopic structure of columnar sea ice-Horizontal section for S2 ice type (*Lainey and Tinawi, 1984*)

The many processes that can occur during the formation and growth of sea ice cause it to assume a variety of crystalline structures. These processes include climatic phenomena (cooling of the water surface and falling of snow) and oceanographic influences (disturbance of the water surface by waves and precipitation of sea salts). The types of crystalline structure, the macrostructure of ice (presence of horizontal bands of ice) and the microstructure of ice (grain size, shape, and c-axis orientation), have a major influence on the mechanical properties of sea ice. Different types of ice are conveniently classified and described in *Table E.1*. This classification was initially intended for river and lake ice, but it can be applied reasonably well to sea ice.

E.2.3 The formation of sea ice

Primary ice formation.

Under very calm sea conditions and relatively low temperature gradients, a very thin, super cooled water layer may appear at the sea surface. The temperature of this layer will actually be several degrees lower than the freezing temperature of seawater. Before ice crystals can form, however, minute centers of crystallization called nuclei must be present. Ice nuclei will form naturally only at very low temperature (-38˚*C* to -42˚*C* in fresh water). Alternatively, nuclei can also be formed by falling snow or atmospheric ice. With such external nuclei, less super cooling is required for ice crystals to form. The amount of super cooling under typical conditions does not normally exceed hundredths of a degree. In such calm, super cooled conditions, ice crystals will grow in the form of needles whose c-axes are parallel to the needle axis and at random orientation to the water surface. These needles will tend to grow along the basal plane into the water. At small temperature gradients, crystallization will proceed at a slow pace, and the needles will float horizontally, the c-axis taking a horizontal orientation. At large temperature gradients, the solidification of the ice cover will occur more rapidly; the initial needles will interlock, and the c-axis will take a random orientation.

In most cases, sea ice will begin to form when wind and waves agitate the surface layer; super cooling will then extend to deeper levels. Natural nucleation will then cause the formation of frazil particles in the form of small discoids. As these grow, they will adhere to each other first to form slush, only to refreeze quickly and form the first layer of ice (primary ice). The crystal orientation in this layer will usually be random.

Secondary ice formation

After the primary ice layer has formed, the salt present in seawater plays a major role in the resulting structure, making it quite different from fresh water ice. Sea ice will grow at a non-uniform rate at the ice-water boundary. In calm conditions, several centimeters of ice at the bottom of the ice sheet consist of pure ice platelets with layers of trapped brine sandwiched between. The c-axis of the plates will be nearly horizontal, and the bearing alignment, will be strongly influence by the direction of the current at the ice and seawater interface. As the freezing progresses, the platelets thicken up, and ice bridges develop between adjacent ones, forming brine cells. The brine cells shrink in size as the ice cools and form the long vertical cylinders that distinguish the structure of this secondary ice form from that of primary ice.

The primary ice layer occupies only the top few centimeters, and the strongly columnar secondary ice can become almost 2 m thick in the Arctic or Antarctic. As mentioned, this layer will show a preferred horizontal c-axis alignment.

Superimposed ice

Superimposed ice frequently occurs on top of primary ice; it can be formed by refreezing of melted ice; freezing of water flooding up in pressure zones, freezing snow that weighs down the ice sheet and is soaked with seawater welling up through cracks. The last ice is called snow (sea) ice as opposed to glacial ice.

E.2.4 The classification of sea ice structures

Both the macrostructure of ice (presence of horizontal bands of ice) and the microstructure of ice (grain size, shape, and c-axis orientation) have a major influence on the mechanical properties of sea ice. Different types of ice are conveniently classified and described in *Table E.1*. This classification was initially intended for river and lake ice, but it can be applied reasonably well to sea ice.

Freshwater ice	Sea ice	Formation condition	Grain size and shape	C-axis
Primary Ice (First to form)				
P1	-	Calm surface, small temperature gradient	Large to extra large size, irregular shape	Preferred vertical
P2	-	Calm surface, large gradient	Medium to extra large size, tabular or needle like shape	From vertical to random
P3	P3b	Nucleation from Frazil	Fine to medium size, tabular shape	Random
P4	P4b	Nucleation from snow	Fine to medium size, equiaxed shape	Random
Secondary Ice (Forms under Primary Ice)				
S1	-	Columnar-grained, forms parallel to heat flow	Large to extra large size, irregular shape	Preferred vertical
S2	S2b	Columnar-grained like S1	Medium to extra large size,	Initial random, then horizontal
S3	S3b	Columnar-grained like S1	Large to extra large size	Preferred horizontal
S4	S4b	Congealed frazil slush	Fine to medium size, irregular shape	Random
S5	-	Drained, congealed frazil slush	Fine to medium size, angular shape	
Superimposed Ice (Forms at top of cover)				
T1	T1b	Snow ice	Fine to medium, round to angular	Random
T2	T2b	Drained snow ice	Fine to medium, rounded shape	Random
T3	T3b	Surface ice	(Layers of columnar ice formed on top of original primary ice)	
Agglomerate Ice				
T3	Rb	Agglomerate ice	(Individual pieces that have refrozen; May be rafted or ridged)	

Table E.1 Classification of ice types
(*Michel and Ramseier, 1971, and Nadreau and Michel, 1984*)

E.3 The density of pure ice

The density of pure ice is usually given as 916.8 kg/m^3 at 0˚*C* from *Dorsey* (*1940*). Later *Butkovich* (*1955*) confirmed this by making very accurate measurements of single crystals at –3.5˚*C*. He got the value 917.28 kg/m^3 which extrapolated to 0˚C by means of the coefficient of thermal expansion gives 916.82 kg/m^3. He also measured the density as a function of temperature and his experiments gave that the volume expansion with temperature is linear with good accuracy between -30˚*C* and 0˚*C*. (*Fig E.5*)
Anderson (*1960*) proposed a constant volume coefficient of thermal expansion (γ) of $1.445 \cdot 10^{-4}$ */K* in this interval which gives good agreement also to other scientists results. The linear coefficient (α) is $4.82 \cdot 10^{-5}$ */K*, that is a third of the constant volume coefficient of thermal expansion (γ). The density as a function of temperature will be given by

$$\rho(\theta) = \rho_o/(1+\gamma\theta) \qquad \text{(E-1)}$$

where $\rho(\theta)$ is the compact density of ice at the temperature θ(˚C),
ρ_o = 916.82 kg/m^3 the compact density of ice at 0˚C,
and γ the volume coefficient of thermal expansion.

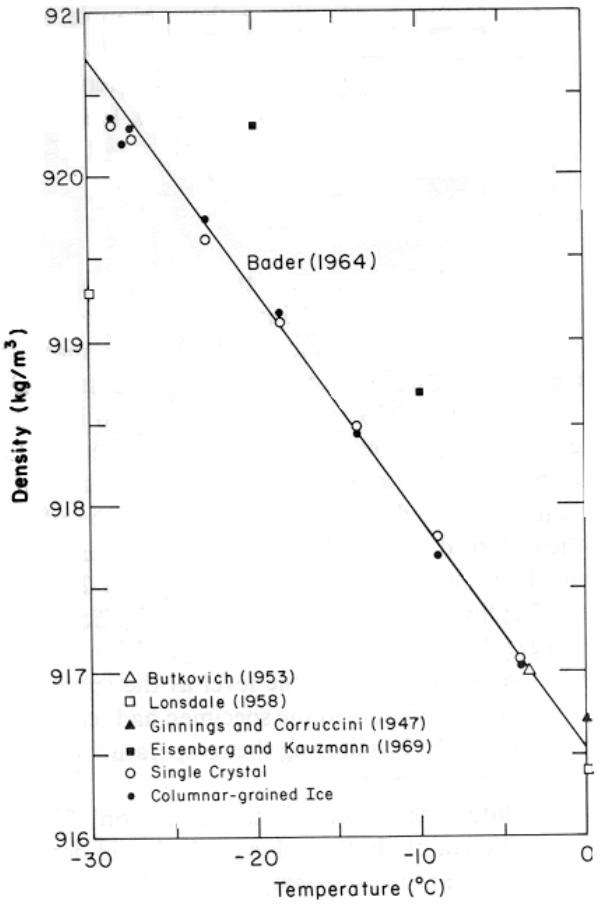

Fig E.5 Density of ice in a temperature range of 0o to-30oC. (after *Hobbs 1974*)

The *Fig A.5* above is the result of measurements from several investigations of columnar-grained freshwater ice (classified as S2 by *Michel and Ramseier 1971*) and was established by using the hydrostatic method. Each point represents the mean value of three to eight measurements. The scatter of the data at a given temperature was about ±0.17 kg/m^3, which was comparable to the estimated possible relative error, ±0.20 kg/m^3.

There was no discernible difference between the densities of single-crystal and columnar-grained ice within the accuracy of the measurements. The density increased almost linearly with decreasing temperature. *Butkovich*'s value (*1957*) was determined by the hydrostatic method for single crystals from a glacier and for commercial ice. The data given by *Lonsdale* (1958) and *Eisenberg* and *Kauzmann* (*1969*) were obtained by determining the unit-cell parameters with X-ray and electron-diffraction measurements (*Hobbs 1974*). *Ginnings* and *Corrruccini*'s value (*1947*) was obtained by the *Bunsen* ice calorimeter. *Bader*'s graph estimate (1964) was based on Butkovich's density data (*1953*) at $-3.5\,^{o}C$ and the thermal expansion coefficient (*Butkovich, 1957*).

E.4 Physical and thermal properties of seawater, sea ice and snow

The following table gives representative physical and thermal properties of seawater, ice, and snow properties. As can be seen the thermal properties of sea ice are especially sensitive to changes in salinity and temperature

Parameter	Value	Ref.
1) Sea water		
Freezing Temperature θ_w (^{o}C)	-1.8 ($S_w = 35$)	(1)
	-1.1 ($S_w = 20$)	
	-0.3 ($S_w = 5$)	
Density at freezing, ρ_w (kg/m^3)	1028 ($S_w = 35$, $\theta_w = -1.8$)	
	1016 ($S_w = 20$, $\theta_w = -1.1$)	
	1004 ($S_w = 5$, $\theta_w = -0.3$)	
2) Sea ice		
Density, ρ_i (kg/m^3)	916.8 ($S_i = 0$, $\theta_i = 0$; fresh water)	(2)
	50-400 (Snow ice)	
	860-920 (First year ice ; winter)	
	830-900 (Multiyear year ice)	
Latent heat of fusion, L (J/g)	334 ($S_i = 0$, $\theta_i = 0$)	
	338 ($S_i = 0$, $\theta_i = -2$)	
	264 ($S_i = 8$, $\theta_i = -2$)	
Thermal conductivity, k_i (W/m^oC)	2.22 ($S_i = 0$, $\theta_i = 0$)	
	2.13 ($S_i = 4.7$, $\theta_i = -5$)	
	2.18 ($S_i = 4.7$, $\theta_i = -15$)	
3) Snow		
Density, ρ_s (kg/m^3)	300-400	(3)
Thermal conductivity, k_s (W/m^oC)	0.25 ($\rho_s = 350$, $\theta = -20$ to -30^{o}C)	

θ = temperature °C, S = salinity ppt.

Table E.2 Representative physical and thermal properties of seawater, ice, and snow.
(1) *Dietrich* and *Kalle*, *1963*,
(2) *Doronin* and *Kheisin*, *1977* and
(3) *Nakawo* and *Sinha*, *1981*.

E.5 References

[1] George D. Ashton: *River and Lake Ice Engineering,* U.S Army, Cold Regions Research and Engineering Laboratory, 1986.

[2] Lars Bergdahl: *Physics of Ice and Snow as Affects Thermal Pressure*, Report Series A:1, Department of Hydraulics, Chalmers University of Technology, Göteborg 1977, pp.7-51.

[3] Norbert Untersteiner, The Geophysics of Sea Ice (1986).

[4] W. F. Weeks and S. F. Ackley, *The Growth, Structure, and Properties of Sea Ice*, 1977, pp.9-164.

[5] Per Tryde, *Physics and Mechanics of Ice* (1980). *IUTAM symposium Copenhagen*, 1979

[6] W Tucker, A Gow, H Bosworth, E Reimmitz, and E Meese, *Sea Ice Characteristics across the Arctic Ocean*, 1994.

[7] T. J. O. Sanderson*, Ice Mechanics* (1988), pp.5-27.

F MECHANICAL PROPERTIES OF ICE

F.1 Introduction

F.1.1 Problems with testing of mechanical properties of ice

Many researchers have investigated the mechanical properties of ice. However the data obtained from supposedly similar tests often differ greatly, or are even contradictory. This unsatisfactory situation arises from the fact that practically every ice research group has its own method for testing the mechanical properties of ice. The anisotropic and visocoelastic features of the ice must be considered together with different test conditions when studying ice properties because neglecting these parameters can cause results to differ from test to test. This means that the mechanical properties of ice are a function of test conditions as well as a basic material property.

F.1.2 Description of general ice strengths

Strength is defined as the maximum stress that a test specimen can support. Furthermore strength is qualified by an associated failure mode, which is a qualitative description of test specimen behavior at maximum stress. Failure is described as ductile when the strain increases in the specimen with no increase stress, and brittle when the specimen ruptures with an instantaneous decrease in stress. Any measure of strain after brittle strength becomes meaningless because of disintegration of the specimen. Strength can thus be qualified as being yield strength or brittle strength. The specification of failure mode must be qualitative since there is no rigorous definition of failure mode.

Relating to strength test, strength values are affected by temperature, ice type, grain size, air bubble content, specimen orientation, loading rate, test system stiffness, end conditions of the specimen, anisotropy, specimen size, and the loading conditions during test.

F.2 The compressive strength

F.2.1 Test methods for compressive strength

Unconfined compression test

Compressive strength of ice is usually obtained from unconfined compression tests on small samples like cylinders, prisms, or cubes. Depending on the sample dimensions, the state of stress varies from three-dimensional at the ends of the specimen to more or less one-dimensional in the central region. The failure is influenced strongly by shear induced by friction at the ends of the specimen.

Confined compression test

Recently a new testing method has been used at the IIHR to obtain a pure uniaxial state of stress in compression tests. A specimen (prism with a height to width ratio of 2.5) is placed between ice blocks with the same cross sectional area – one on top and one underneath the specimen. The height of these additional ice blocks is 0.3h where h is height of the sample to be tested. The advantage of using this method of testing is that, when under compression, the material just above and below the contact surfaces between the heads and the specimen will expand the same amount, since they are of the same material composition.

F.2.2 Compressive strength of pure ice

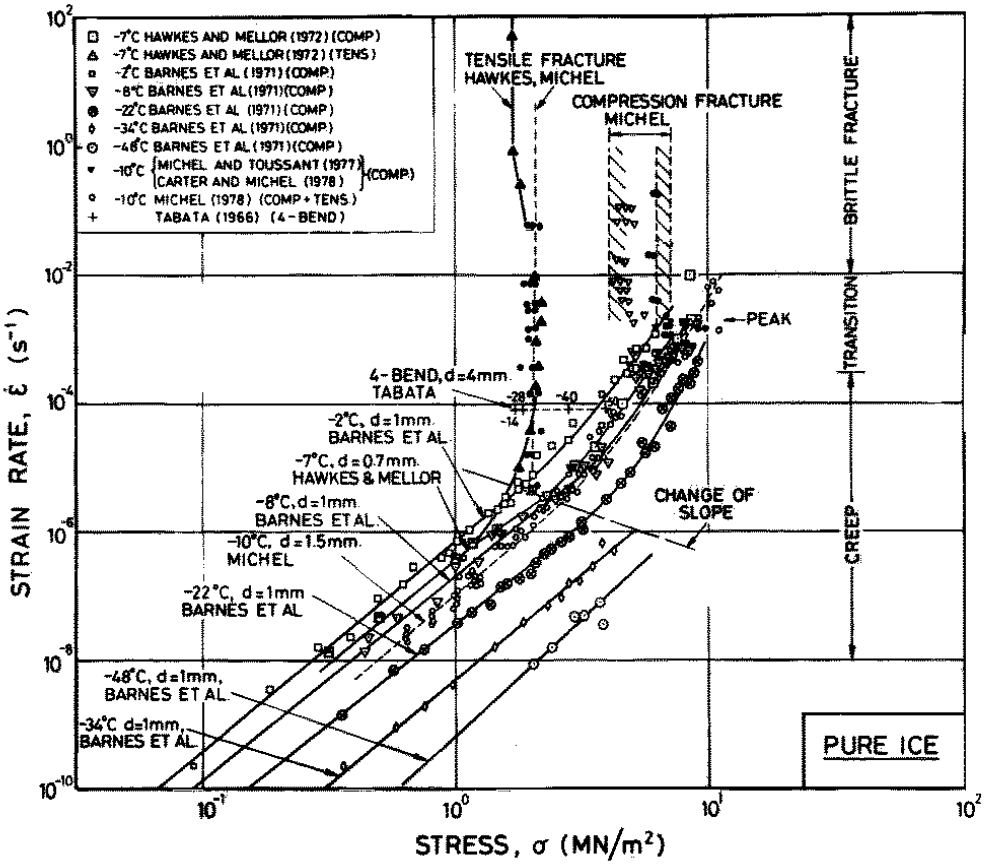

Fig F.1 Stress against strain rate under uniaxial loading of pure polycrystalline ice (after *Hallam, 1986*)

F.2.3 Compressive strength comparison of various ice types

	Columnar Grained Freshwater Ice	Snow Ice	Sea Ice*
Strength (MPa) 0 °C	3.0	3.0	3.0
-10 °C	8,7	3.0	3.0
-20 °C		3.0	3.0
Strain rate (s^{-1})	10^{-3}	10^{-2}	10^{-3}
Sample dimension	4 x 6 x 8 cm	-	10 x 10 x 10 cm
Crystal dimension (mm)	0.4	0.1	< 5
Load relative to growth direction	Perpendicular	Random	Perpendicular
Reference	*Wu, Chang and Schwarz*	*Hawes and Mellor*	*Schwarz*

* The salinity of the water was 12 ‰.

Table F.1 Examples of compressive strength of various ice types

F.2.4 Compressive strength of sea ice

The compressive strength of sea ice varies with strain rate, temperature, porosity, grain orientation, ratio of grain size to specimen size and scale effect between specimen size and prototype.

Unconfined compressive strength of sea ice

- *Butkovich (1956, 1959)*: S2 ice type
  Vertical compressive strength: 7.6 MPa at –5°C, 12.0 MPa at –16°C
  Horizontal compressive strength: 2.1 MPa at –5°C, 4.2 MPa at –16°C

- *Weeks* and *Assur (1967)*:

$$\sigma_c = 1.65\ (1-\sqrt{\frac{\upsilon_b}{275}}\ ) \qquad \text{(F-1)}$$

  where σ_c is in MPa and υ_b is in ‰.

- *Nadreau* and *Michel (1984)*: T1b and S2b ice types
  Maximum yield compressive strength: 7.2 MPa for a strain rate of around 10^{-3} s^{-1}.

- *Timco* and *Frederking (1986)*: S2 ice type
  Horizontal compressive strength: from the work of *Sinha (1983a, 1984*) and *Frederking and Timco (1980,1983,1984a)*

$$\sigma = 39\ (\dot{\varepsilon}_n)^{0.26}(1-\sqrt{\frac{\upsilon_t}{320}}\ ) \qquad \text{(F-2)}$$

  Vertical compressive strength: from the work of *Sinha (1983b)* and *Frederking* and *Timco (1980,1984a)*

$$\sigma = 150\ (\dot{\varepsilon}_n)^{0.22}(1-\sqrt{\frac{\upsilon_t}{280}}\ ) \qquad \text{(F-3)}$$

  where σ is in MPa; the nominal strain rate, $\dot{\varepsilon}_n$, in s^{-1} such that $10^{-5} \geq \dot{\varepsilon}_n \geq 10^{-3}$; and υ_t, the total porosity, in ‰. Comparison of these unconfined tests indicated that the strength of this ice loaded vertically is approximately four times higher than its strength loaded horizontally.

Confined compressive strength

- *Timco* and *Frederking (1984)*:
  The data were presented from tests using three different confinement arrangements for specimens.
  Type-A: horizontal loading with vertical confinement
  Type-B: horizontal loading with horizontal confinement

$$\sigma = 55\ (\dot{\varepsilon}_n)^{0.46} \qquad \text{(F-4)}$$

Type-D: vertical loading with vertical confinement

$$\sigma = 8.9\ (\dot{\varepsilon}_n)^{0.26} \qquad \text{(F-5)}$$

where σ is in MPa and the nominal strain rate, $\dot{\varepsilon}_n$, in s^{-1} such that $10^{-5} \geq \dot{\varepsilon}_n \geq 10^{-3}$.

As the conclusion, confinement conditions do not appreciably affect the strength of the ice if the confinement is of either B or D type. For A-type confinement, the stress level can be over four times higher than the strength of the ice with no confinement (see the equation *F-2*).

F.3 Tensile Strength

F.3.1 Test methods of tensile strength

The tensile strength of ice can be measured only by direct tension tests. Ring tensile tests (indirect test), which have been extensively applied to the studies of sea ice by American and Canadian investigators do not provide the true tensile strength because the stress state is complex and the failure is restricted to a very small and unpredictable volume of the specimen. This testing method has, however, the advantage that the sample preparation and testing are easy and can be used to investigate qualitatively the effects of certain parameters like salinity and temperature on the tensile strength. The absolute values, however, are unlikely to be the tensile strength and only a limited amount of direct tensile strength data is available.

F.3.2 Tensile strength of pure ice

Such as compression, tensile strength can be associated with either brittle or ductile failure. In the range of brittle behavior (strain rates greater than $10^{-6}\ s^{-1}$), strength appears to be a function primarily of grain size and to a much lesser extent, of temperature. The effect of strain rate on the tensile strength of pure ice is very small in comparison with effect on the compressive strength. For tensile strength in the brittle range, *Michel (1978)* proposed the following equation

$$\sigma = 7.94 \times 10^4 \left[(1 - e/0.285)(1 - 0.9 \times 10^{-3}\theta)/d \right]^{1/2} \text{Pa} \qquad \text{(F-6)}$$

where e = porosity $(1-\rho'/\rho)$, ρ = density of pure ice (917 kg/m^3), ρ' = density of the ice (kg/m^3), θ = temperature (℃), d = grain diameter (m). This equation is supported by data for grain sizes ranging from1.4 to 9 mm and the variation in tensile strength with temperature is much less than the variation of compressive strength.

In the region of ductile failure, the yield tensile strength is reported as being the same as the compressive strength up to a transition strain rate. That rate appears to be a function of temperature and grain size and no investigations have been made so far concerning scale effects on determination of the tensile strength of ice.

F.3.3 Tensile strength of sea ice

- *Dykins (1970)*: S2 ice type, at a constant strain rate of 6.3 x 10^{-3} s^{-1}.
  Vertical tensile strength:

$$\sigma_t = 1.54\ (1 - \sqrt{\frac{\upsilon_b}{311}}) \qquad \text{(F-7)}$$

Horizontal tensile strength:

$$\sigma_t = 0.82\ (1 - \sqrt{\frac{\upsilon_b}{142}}\ ) \qquad \text{(F-8)}$$

where the tensile strength, σ_t, is in MPa and the brine volume, υ_b, in ‰.

Dykins (1970) stated that tensile strength was not appreciably dependent on the crystal size or on the stress rate in the range of 1 kPa /s to 0.18 MPa /s. For stress rates greater than 0.18 MPa /s, however, the tensile strength decreased by 52 % of its initial value. *Dykins'* results showed that the ice was two to three times stronger when the tension was applied in the vertical direction rather than in the horizontal.

- *Saeki, Normura*, and *Ozaki (1978)*: S2 ice type, at -7°C to -2°C for salinities of 3.8 to 6.5 ‰ and stress rates of 60 to 1200 kPa /s.
  When the load is applied perpendicular to the grain structure:

  $$\sigma_t = 95 + 50\,(-\theta) \qquad \text{(F-9)}$$

  where the tensile strength, σ_t, is in kPa and θ is in $°C$.

F.4 Flexural strength

F.4.1 Test methods of flexural strength

Flexural strength (Bending strength) is used in applying to such problems as measuring ice breaker performance, determining ice forces on inclined structures, understanding ridge-building and rubble-building processes, and determining safe bearing capacities of ice covers. Flexural strength is commonly obtained from simple beam tests, cantilever beam tests, four-point loading and plate loading tests. The stress calculation in these cases is based on elastic theory.

Since the elastic theory does not consider the viscoelastic and anisotropic properties of ice, the flexural strength, even though it is not one of the basic material properties, cannot be calculated properly by this method. Instead of using the elastic constants for calculating the bending strength, the strain modulus should be applied.

F.4.2 Basic description of flexural strength

The flexural behavior of ice covers is important in establishing their bearing capacity or for determining their loads on inclined structures. Flexural strength is not a basic material property but should be considered as an index value. It may be calculated as follows:

$$\sigma_f = \frac{6M}{bh^2} \qquad \text{(F-10)}$$

where σ_f is the flexural strength; M, the maximum moment resistance; b, the beam width; and h, the beam depth. This equation assumes that the deformation is elastic and that the material is homogeneous and isotropic.

F.4.3 Flexural strength of sea ice

- *Määtänen (1976)*
  Found a decrease in strength and modulus with increasing ratio of beam width to ice thickness.
- *Frederking* and *Hausler (1978)*
  Found that buoyancy effects could be ignored if the ratio of beam length to ice thickness was less than 10.
- *Frederking* and *Timco (1983)*
  Showed that flexural strength was independent of beam length but decreased with increasing beam width.
  Showed that flexural strength was independent of loading rate but that the modulus decreased with increased loading time.
- *Nadreau* and *Michel (1984)*: in-situ cantilever beam tests with lengths between 140 and 27,000 mm, temperature between -1.7°C and -12°C, salinities between 5.0 to 19.0 ‰ and stress rates between 3 and 3200 kPa /s.
  For $\upsilon_b^{1/2} < 0.33$ ($\approx \upsilon_b < 0.109$ ‰):

$$\sigma_f = 0.75\ (1 - \sqrt{\frac{\upsilon_b}{0.202}}) \qquad \text{(F-11)}$$

  where the σ_f is in MPa and and υ_b is the brine volume divided by 1000.
- Dykins (1971): in-situ beams with ice thickness of up to 2.4 meters.

$$\sigma_f = 1.03\ (1 - \sqrt{\frac{\upsilon_b}{0.209}}) \qquad \text{(F-12)}$$

  where the σ_f is in MPa and and υ_b is the brine volume with values up to 0.012 (12.‰)

F.5 Shear Strength

F.5.1 Test methods of shear strength

Shear is characterized by lateral movement (that is angular distortion) within a material. Torsion, direct shear and punching are the main methods of generating shear stresses. In all these methods rather arbitrary assumptions are made about the shear plan. Therefore, it is difficult to compare the strength results of various investigators. This means that amount of information available on the shear strength of ice is quite limited because of the lack of information on ice types, loading rates, experimental arrangement, etc. In addition, many of the data described as shear strength are the result of mixed failure modes. Although there are several weaknesses in information of test results relating to shear strength of ice, we can roughly consider the following facts; a) A considerable influence of the sample size was observed for high loading rates only; b) The shear strength decreases with the loading rate even for ductile deformation range; c) The temperature seems to has no influence on the shear strength.

F.5.2 Shear strength of sea ice

- *Butkovich (1956)*: from sea ice that salinities ranged from 3.7 to 7.9 ‰ and the loading rate varied between 30 to 150 kPa /s.

Shear strengths 0.8 to 3.4 MPa were reported, with an average value around 2.1 MPa.

- *Serikov (1961)*: at air temperature between –0.9 and –4.1°C.
  Showed the average value was 0.9 MPa by punching shear tests.
- *Dykins (1971)*: from sea ice that salinities ranged from 1.0 to 9.0 ‰ at temperature between –4.0 and –27.0°C.
  Showed an average value was between 140 and 350 kPa.
- Pounder and Little (1959), Frederking and Timco (1984): used an asymmetrical four-point bending test with 4.2 ‰ salinity at a temperature of –13.0 °C.
  Reported a value of shear strength for granular ice was 500 kPa.

F.6 Elastic modulus

F.6.1 Test methods of elastic modulus

There are two methods to determine the elastic modulus: the static method using *Hooke*'s law and seismic (dynamic) method supplying the elastic modulus by measuring the propagation velocity of longitudinal and transverse elastic waves. The latter method provides the most accurate value of the elastic constants.

F.6.2 Basic description of elastic modulus

The elastic behavior of homogeneous and isotropic material is described by two independent elastic constants. Many more constants are in use, so it is possible to calculate each of those suing two others. Well-known constants are the bulk modulus (K), *Young*'s modulus (E), the shear modulus (G), *Lame*'s constant (λ), and *Poisson*'s ratio (ν). These elastic constants are only defined for isotropic bodies. Ice is only isotropic if the orientations of the c-axes of the ice crystals are random. If the distribution is not random, it is difficult to describe the elastic behavior completely.
The following data are the results of several researchers.

Author	Method	Type of ice	Temperature (°C)	Bulk modulus K (GPa)	Shear modulus G (GPa)	*Young*'s modulus E (GPa)	*Poisson*'s ratio (ν)
Brockamp and Reuter (1969)	Voigt	Lake ice	-20.5	8.5	3.6	9.5	0.314
Brockamp and Reuter (1969)	Reuss	Lake ice	-20.5	8.5	3.5	9.2	0.319
Brockamp and Querfurth (1965)	Ultra-sound	Artificial Ice	-0.5		3.1	8.5	0.346
Brockamp and Kohnen (1967)	Seismic	ice cap (Greenland)	-19.0	8.8	3.4	8.9	0.330
Brockamp	Seismic	ice cap		9.9 – 10.4		8.4	0.345
Nakaya (1958)	Reso-nance	ice cap				9.4	

Table F.2 Elastic constants of polycrystalline ice

F.6.3 Elastic modulus of sea ice

Dynamic measurements

The value of modulus determined by this method is based on the rate of propagation of vibrations in the ice or by exciting resonant frequencies in small-scale specimens. The displacements in such measurements are extremely small, and anelastic effects can be neglected. Normally two main approaches have been used to obtain dynamic determinations of E for sea ice.

Seismic field techniques

- *Kohnen (1972)*
  Found E varying from 1.7 to 5.7 GPa when measured by flexural waves and 1.7 to 9.1 GPa when determined by in-situ body-wave velocities.
- *Peschanskii (1960)*
  Showed that as the temperature of the ice increased, the ice thickness decreased and the values of E showed a pronounced decrease.

Small-specimen techniques

- *Tabata (1959)*: obtained the natural resonance frequency of sea ice bars with 0.02 x 0.035 x 0.35.

$$E / E_0 = 1 - (\upsilon_t / \upsilon_0) \qquad \text{(F-13)}$$

  where E_0 is the sonic modulus of pure ice; υ_t, the total porosity (brine and air); and $\upsilon_{0,}$ the υ axis intercept (180-220 ‰).

- *Langleben* and *Pounder (1963)*: from 300 samples of cold Arctic sea ice

$$E = 10.0 - 3.51\upsilon_b \quad \text{(Gpa)} \qquad \text{(F-14)}$$

  where υ_b is the brine volume divided by 1000 (‰).

Static measurements

The static tests measure strain after the application of a load and thus the deformation can be measured only after a finite time interval. Because of the viscoelastic behavior of ice, this interval is invariably sufficient to permit viscous, as well as the desired elastic, deformation. Therefore, a static modulus determination specified by the measurement of total deformation does not characterize the resistance of ice to an instantaneous elastic deformation. The greater the stress, the more important the viscous and creep components become. Hence, the value of the modulus calculated on the basis of strain measurements decreases as stress increases.

- *Lainey* and *Tinawi (1980)*
  Found that the effective elastic modulus increased linearly with decreasing temperature and appeared to reach a constant value at stress rates greater than 100 kPa /s. Average values for ice of 5 ‰ salinity ranged from 3.5 GPa at -5°C to 6.5 GPa at –40 °C.
- *Cox et al. (1984)*: by samples from multiyear ice ridges in the Beaufort Sea.
  5.02 GPa to 6.99 GPa at strain rates of 10^{-5} and 10^{-3} s^{-1} at –5°C.
  5.95 GPa to 7.62 GPa at strain rates of 10^{-5} and 10^{-3} s^{-1} at –20°C.

F.7 Poisson's ratio of sea ice

- *Weeks* and *Assur (1967)*

$$\nu_D = 0.333 + 6.105 \times 10^{-2} \exp(-\frac{T}{5.48}) \quad \text{(F-15)}$$

where the ν_D is the dynamic Poisson's ratio and T is the ice temperature in °C.

- *Murat* and *Lainey (1982)*

$$\nu = 0.24(\frac{\dot{\sigma}}{\dot{\sigma}_1}) + \nu_D \quad \text{(F-16)}$$

where $\dot{\sigma}_1$ is a unit stress rate (1 kPa /s).

- *Mellor (1983)* at very low stress rates

$$\nu_e = \left(\frac{1}{2}\right) - \left(\frac{1}{6}\right)\left(\frac{E}{E_0}\right) \quad \text{(F-17)}$$

where the ν_e is the effective *Poisson*'s ratio; E, the effective *Young*'s modulus; and E_0, the true *Young*'s modulus for zero porosity.
At the highest test rates ($\dot{\sigma}$ = 0.6 MPa /s and $\dot{\varepsilon}$ = 1.6 x 10^{-4} s^{-1}), ν had values between 0.35 and 0.4.

- *Saeki, Ozaki*, and *Kubo (1981)*: for radial expansion of vertical cylinders
Showed that ν varied between 0.02 and 0.48.
- *Wang (1981)*
Showed that ν varied between 0.8 and 1.2 in the horizontal direction and 0 to 0.2 in the vertical direction.

Although values of *Poisson*'s ratio around 1/3 seem to be appropriate for elastic deformations, the effect of anisotropy and confinement on columnar sea ice need be investigated for viscoelastic deformation.

F.8 Adhesion strength of sea ice

The important parameters influencing on bond strength of ice are roughness, interface temperature, and salinity of ice.

- *Sackinger* and *Sackinger (1977)*: from sea specimens that salinities ranged from 0.4 to 20 ‰ over the range of –1.5 to –23.0°C.
The values of bond strength were between 250 kPa to 1.7 MPa.
- *Oksanen (1983)*: by push down tests on steel plates that salinities ranged from 1.6 to 1.8 ‰ at a temperature of -10°C.
The values of bond strength were between 23 kPa to 253 kPa.

F.9 Fracture toughness

Fracture toughness or critical stress intensity factor is a material property that determines the stress necessary to propagate a crack of known size.

- *Vaudrey (1977)*: by using a four-point bending test for saline ice with a brine volume between 18 to 40 ‰ at temperature of –10 to –20°C.
  The values of the critical stress intensity factor (K_{IC}) were between 28 and 126 kPa $m^{1/2}$.
- *Urabe, Iwasaki*, and *Yoshitake (1980)* and *Urabe* and *Yoshitake (1981a, 1981b)*: by using a three-point bending test for sea ice of grain size between 3 and 30 mm at temperature of –2°C.
  Reported that the average value of the critical stress intensity factor (K_{IC}) was 70 kPa $m^{1/2}$.
- *Timco* and *Frederking (1983)*: by using a four-point bending test for sea ice at a loading rate of 10 kPa $m^{1/2}$/s and at a temperature of of –20°C.
  For salinity ranged between 4 and 7 ‰, K_{IC} was constant at about 110 kPa $m^{1/2}$ and between 3 and 5 ‰, K_{IC} increased to about 145 kPa $m^{1/2}$.

F.10 References

[1] A. B. Cammaert and D. B. Muggeridge, *Ice Interaction with Offshore structures* (1988), pp.76-120.

[2] T. J. O. Sanderson, *Ice Mechanics* (1988) Laboratory Studies, pp.70-103.

[3] Lars Bergdahl, *Physics of Ice and Snow as Affects Thermal Pressure* (1977), pp.100-139.

[4] George D. Ashton, U.S Army Cold Regions Research and Engineering Laboratory, *River and Lake Ice Engineering* (1986), pp.50-85.

[5] Norbert Untersteiner, *The Geophysics of Sea Ice* (1986)

[6] W. F. Weeks and S. F. Ackley, *The Growth, Structure, and Properties of Sea Ice* (1977), pp.9-164.

[7] Malcolm Mellor, *Mechanical Behavior of Sea Ice* (1977), pp.165-281.

[8] Per Tryde, *Physics and Mechanics of Ice* (1980). IUTAM symposium Copenhagen 1979

[9] G. A. Kuehn and E. M. Schulson, *The mechanical properties of saline ice under uniaxial compression*, (1994), pp.39-48.

[10] G. A. Kuehn, E. M. Schulson, D.E. Jones, and J.Zhang, *The compressive Strength of Ice Cubes of Different Size*, (1993).

[11] Lau, P. A. and C.M. Browne, *Bending and compression properties of young sea ice*. In OCEANS'80 (1989).

[12] Jon E. Zufelt and Robert Ettema, *Model Ice Properties*. CRREL Report 96-1 (1996).

[13] Austin Kovacs, *Estimating the full-scale Tensile, Flexural and Compressive Strength of First-Year Ice*, CRREL Report 96-11(1996).

G ICE FORCES ON VERTICAL STRUCTURES

G.1 Introduction

G.1.1 Idealized failure mode

Idealized failure modes associated with ice features interacting with vertical structures include crushing failure, flaking failure, bending failure in the horizontal plane, buckling, shear failure in the vertical plane, and fracture failure. The irregularity of the properties and morphology of ice features make the assumption of a single failure mode questionable, particularly for the case of wide structure, where several failure modes may be in effect at the same time (*Kry, 1978*).

G.1.2 Various failure modes

- Crushing failure is a rather complete disintegration of the ice by numerous cracks into a rubble field that offers no appreciable further resistance.
- Shear failure is a flaking of the ice along failure planes at angles near 45˚ upwards or down wards.
- Buckling failure is the formation of one or more cracks at some distance from the structure by a combination of bending and compression.
- Cleavage failure occurs when a horizontal cleavage crack of the ice sheet near the structure precedes one of the three crack patterns above.

G.1.3 Failure for various ice types

Sheet ice failure

Sheet ice may fail by crushing of the ice in the area of contact, by buckling of the ice sheet, or by fracture.

- *Sodhi* and *Nevel (1980)*
  The occurrence of crushing or buckling failures depends on the aspect ratio, *D/h*, where *D* is the width of the structure and h is the thickness of the ice sheet. Buckling occurs for aspect ratios generally greater than 6, whereas a crushing failure is characteristic for a *D/h* of less than 6. Failure by fracture depends on the speed of the ice movement and the presence of flaws which may propagate.

First year and multi year ridge failure

First year and multi year ridges and rubble piles may fail by crushing of the ice in the area of contact, by bending in the horizontal plane and by shear on vertical planes. The occurrence of these modes depends on the dimensions and cross section of the ridge and on the degree of consolidation.

G.2 Crushing failure

G.2.1 General description of crushing failure

Crushing is the most common failure modes for ice interacting with narrow vertical structures. These structures include column-supported structures, as well as bridge piers and lighthouses. The crushing failure mode of interaction follows the indentation problem, where a triaxial state of stress develops in the ice due to the confinement effect of the ice sheet in the load application area. Limiting cases of the state of stress are the plane stress and plane strain cases. Plane stress is approached as the ratio of the indentor width (*D*) to the ice thickness (*h*) approaches infinity, causing the stress in the vertical

direction to approach zero. The plane strain case occurs where the strain in the vertical direction approaches zero as *D/h* approaches zero.

G.2.2 Force exerted due to crushing failure

$$F_c = pDh \tag{G-1}$$

where F_c = the failure load, p = the effective ice pressure, h = ice thickness, D = the width of the indentor.

Empirical approach

The effective ice pressure is related to the uniaxial compressive strength by a number of coefficients that each has a physical interpretation.

- Korzhavin's (1962)

$$p = If_c m \left(V/V_0\right)^{-0.333} \sigma_C \tag{G-2}$$

where I is the indentation coefficient to account for confining effects (if the ice width is greater than 15D, then I = 2.5), f_c is the contact factor which accounts for non-simultaneous contact between the indentor and the ice, m is the shape factor, V is the velocity of the ice sheet, V_0 is the reference velocity of 1 *m/s*, and σ_c is the unconfined compressive strength of the ice.

Indentor width (m)	Value of f_c at ice velocities (m/s) of		
	0.5	1.0	2.0
3 - 6	0.7	0.6	0.5
6 - 10	0.6	0.5	0.4

Table G.1 Values of the contact coefficient f_c as a function of indentor width and ice velocity. (From *Korzhavin 1962*)

- *Neill (1976)*
  Korzhavin's formula is valid for strain rates of 10^{-3} to 10^{-4} and gives values of the effective pressure in the range of $0.9\ \sigma_c < p < 1.6\ \sigma_c$.
- *Korzhavin*'s general equation for all strain rates

$$p = If_c m \sigma_C \tag{G-3}$$

- *Michel* and *Toussaint (1977)*: columnar (S2) fresh water ice (*Fig C.1*)
  For the ductile zone:

$$p = If_c m \sigma_{c\max} \left(\dot{\varepsilon}/\dot{\varepsilon}_0\right)^{0.32} \quad \text{for } 10^{-8} < \dot{\varepsilon} < 5 \cdot 10^{-4}\ s^{-1} \tag{G-4}$$

where I = 2.97, f_c = 1.0 for full contact and 0.6 for continuous crushing or initial incomplete contact, m = 1.0 for a rectangular indentor, $\dot{\varepsilon}_0 = 5 \cdot 10^{-4}\ s^{-1}$.

For the transition zone:

$$p = If_c m \sigma_{c\max} \left(\dot{\varepsilon}/\dot{\varepsilon}_0\right)^{-0.126} \quad \text{for } 5 \cdot 10^{-4} < \dot{\varepsilon} < 10^{-2}\ s^{-1} \tag{G-5}$$

where $I = 2.97$, $f_c = 0.25$ for full contact and 0.6 for continuous crushing or initial incomplete contact, $m = 1.0$ for a rectangular indentor, $\dot{\varepsilon}_0 = 5 \cdot 10^{-4}\ s^{-1}$.
For the brittle zone:

$$p = If_c m\sigma_{cb} \quad \text{for } \dot{\varepsilon} > 10^{-2}\ s^{-1} \tag{G-6}$$

where $I = 3$, $f_c = 0.3$, $m = 1.0$ and σ_{cb} = the uniaxial crushing strength under brittle conditions.

The definition of $\dot{\varepsilon} = V/4D$ is a matter of convenience, as the strain rate varies behind the indentor. *Fig G.1* is the relation between uniaxial crushing and indentation strength of S2 ice from *Michel* and *Toussaint*. To convert indentor or ice velocity to strain rate, the velocity must be divided by a length. This length is related to the size of the zone of ductile deformation in front of the indentor. Temperature is also affects ice strength.

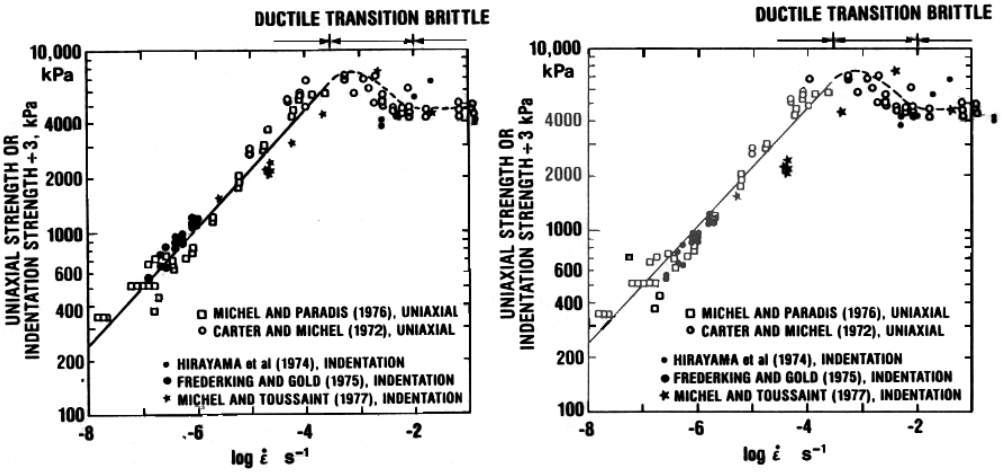

Fig G.1 Uniaxial crushing and indentation strength of S2 ice at –10 ^oC *(Michel* and *Toussaint, 1977)*

- *Ralston (1978*): proposed the expression $\dot{\varepsilon} = V/2D$
- *Palmer et al. (1978)*: proposed the expression $\dot{\varepsilon} = V/D$ as convenient parameters for stain rate representation.
- *Bohon* and *Weingarten (1985)*

$$\begin{aligned} &\dot{\varepsilon} = V/4D \text{ for } 0.5 > D/h \\ &\dot{\varepsilon} = VD/h^2 \text{ for } 0.5 \le D/h \le 2.0 \\ &\dot{\varepsilon} = 2V/h \text{ for } 2.0 < D/h \end{aligned} \tag{G-7}$$

- *Schwarz (1979*): Temperature effect for ice crushing strength. Under the same conditions of test, the lower temperature, the higher strength of ice

G.2.3 Theoretical approach

The indentation problem is applied the plasticity theory bound solutions.

- *Croasdale et al. (1977)*

$$p = I\sigma_C \qquad \text{(G-8)}$$

where I = the indentation factor which can be determined from upper and lower bound solutions. The expression assumes perfect contact between the structure and the indentor.

For rough contact: $I = 1.45 + \dfrac{0.35}{D/h} \leq 2.57$ (G-9)

For smooth contact: $I = 1.15 + \dfrac{0.37}{D/h}$ (G-10)

The application was granular ice and the assumptions ere that the ice was homogeneous and isotropic (*Tresca* yield criterion) and an elastic perfectly plastic material, that the strength of the ice was equal in tension and compression, and that it was not sensitive to hydrostatic pressure.

- *Ralston (1978)*: used the *von Mises* criterion to analyze randomly oriented columnar ice.
- *Ponter et al. (1983)*: proposed reference stress method for low strain rate problems and fracture analysis for high strain rate problems
- *Walden et al. (1987)*: proposed impact model in which the kinetic energy of the floe is dissipated in the failure of the ice.

G.2.4 Shear failure

Croasdale et al. (1977) proposed a model for this case based on plastic limit theory with the shear failure mechanism and a *Tresca* material with $\tau / \rho = 0.5$ at yield conditions. Their formula for the frictionless indentor is

$$p / \sigma = 1 / \cos\theta \ \ (h / 4D + 1 / 2\sin\theta) \qquad \text{(G-11)}$$

The critical angle θ is the one giving a minimum p / σ. If $\partial(p/\sigma) / \partial(\theta) = 0$, the angle can be determined as a function of b/h. Now θ turns out to be close to 45^o, and if this value is inserted, equation above becomes

$$p / \sigma = 1.0 + 0.35\ h/D \qquad \text{(G-12)}$$

which is referred to as the *Morgenstern - Nuttall* formula.

If there is friction or adhesion between the ice sheet and the indentor, the ice pressure is increased. The worst case is adhesion with an adhesive strength equaling or exceeding the shear strength. In that case the pressure becomes

$$p / \sigma = \sec\theta\ \mathrm{cosec}\theta + h\ \tan\theta\ \mathrm{cosec}\theta / 4D + \cot\theta/2 \qquad \text{(G-13)}$$

G.3 Buckling failure

Sodhi and *Hamza (1977)* suggested the buckling load *(F_b),* when distributed over a structure width *(D),* as

$$F_b = kl^3\left[(D/l) + 3.32\left(1 + (D/4l)\right)\right] \quad \text{(G-14)}$$

where k represents the foundation modulus (equal to the weight density of water), l is the characteristic length, $\left[Eh^3/12(1-\nu^2)k\right]^{0.25}$, D is the width of structure, E is the elastic modulus of ice, and v is the *Poisson*'s ratio.

G.4 Splitting failure

- *Michel (1978)*
  The splitting failure occurs most commonly when an intermediate-size floe which is not big enough to be stopped by a structure, nor to be crushed, is split along a line of minimum resistance.

G.5 Cleavage failure

The failure processes can be described by relatively few universal, nondimensional variables. In particular the aspect ratio D/h seems to explain variations in both D and *h.* The description of cleavage failure seems more difficult in this respect. The formulas proposed so far can be written

$$p / \sigma = C\, D^{\alpha}\, h^{\beta} \quad \text{(G-15)}$$

where C must have the dimension (length)$^{-(\alpha+\beta)}$. *Table G.2* lists the numerical values of C, α and β given by various researchers.

	Shape of indentor	C	α	β	Mode of failure
Saeki and Osaki (1980)	flat	6.8	-0.50	0.0	Cleavage
	circular	5.0			
	wedge	4.5			
Schwarz et al. (1974)	circular	3.57	-0.50	0.10	Cleavage
	flat	6.8			

Table G.2 Constants used to determine the ice pressure required for cleavage failure

G.6 Vertical lifting failure

- *Christensen* and *Tryde (1984)*
  In areas of frequently varying water level, vertical ice lifting forces play an important role in the failure of vertical structures. The maximum uplift force for bending failure of the surrounding ice sheet is given as

$$F_v = 1.54\sigma_f h^2\left(1.05 + 2\alpha + 0.5\alpha^3\right) \quad \text{(G-16)}$$

where σ_f is the flexural strength of ice, h is the ice thickness, and α is the nondimensional pile radius (r/l), where r is the radius of the pile and l is the characteristic length.

An upper limit to uplift or down-drag forces are provided by the adhesion bond between the ice and the structure. In some cases, a thick adfreeze shear strength may limit vertical forces. The limit force for both situations is calculated from

$$F_a = \tau S \tag{G-17}$$

where τ is the adfreeze shear strength, and S is the adfreeze area($S = 2\pi rh$).

G.7 References

[1] A. B. Cammaert and D. B. Muggeridge*, Ice Interaction with Offshore structures* (1988), pp.225-246.

[2] George D. Ashton, U.S Army Cold Regions Research and Engineering Laboratory, *River and Lake Ice Engineer*ing (1986), pp.125-146.

[3] Per Tryde, *Physics and Mechanics of Ice* (1980). IUTAM symposium Copenhagen 1979.

[4] Stefan Karlsson and Peter Strindö, *Ice Forces on Cylindrical and Conical columns* (1985).

[5] Juri Kajaste-Rudnitski, Pauli Jumppanen, and William M. Sackinger, *Ice Loads upon a Cylindrical Offishore Structure* (1985).

[6] Austin Kovacs, *Estimating the full-scale Tensile, Flexural and Compressive Strength of First-Year Ice*, CRREL Report 96-11(1996).

[7] A. W. Lipsett, *Field Measurements of Ice Forces on Bridge Piers* (1973-1979).

[8] K. Kato and D. S. Sodhi, *Ice Action on Pairs of Cylindrical and Conical Structure* (1983), CRREL Report 83-25.

[9] Mauri Määttänen, *On Conditions for the Rise of Self-excited Ice-induced Autonomous Oscillations in Slender Marine Pile Structures*. (1978).

[10] T. Carstens, *Working Group on Ice Forces on Structures* (1980).

[11] Ken-ichi Hirayama, Joachim Schwarz, and Han-chin Wu, *An Investigation of Ice Forces on Vertical Structure* (1974).

H ICE FORCES ON SLOPING STRUCTURES

H.1 Introduction

H.1.1 Advantage in failure comparing to vertical structure

The advantage of sloping and cone-shaped structures is that they induce bending failure in the ice sheet and hence are subjected to substantially lower loads as compared to the case where the ice sheet fails by crushing on vertical structures.

H.1.2 Various failure modes

As an ice sheet approaches a sloping structure, at first contact the ice begins to crush at the interface. As driving forces increase, the ice continues to crush and the magnitude of the applied forces increases. The interaction force, acting normal to the face of the structure, has a vertical and a horizontal component; the vertical component produces bending in the ice sheet. The ice will fail in bending when the vertical component increases to a certain level. After the local failure of an ice sheet the smaller pieces of ice are pushed by the approaching ice sheet and begin to fide up the face of the structure. This cases a larger interaction force to be generated, since additional force is required to push the broken pieces of ice up the structure. In addition to the predominant mode of bending failure, it is also necessary to consider adfreeze forces that may arise if an ice sheet has developed a bond with the structure during a period of no ice movement. Shearing failure is also possible depending on the relative strength of the ice sheet under vertical and horizontal loading. Bucking of the ice sheet may occur if the ice sheet is think, and there is sufficient resistance to ice movement up a slope.

In most cases of ice forces exerted by horizontally moving ice sheets, the load is determined by that required to fail the ice, so a common design concept is to slope the structure at water line to induce a bending failure rather than a crushing failure. The expectation, of course, is that the load causing failure in bending will be less than the load associated with crushing failure. So the forces on sloping structures are analyzed with two practical goals: to determine the angle of slope needed to induce bending rather than crushing failure and to determine the magnitude of the loads.

H.2 Two-dimensional flexural failure

H.2.1 Process of failure

In the simple two-dimensional model shown in *Fig H.1*, the forces acting on the ice can divided by gravity force (*V)* and buoyancy (*H)*; the buoyancy can be analyzed as an elastic foundation. As the ice sheet first encounters the sloping structure, local crushing occurs on the bottom of the ice sheet. As the ice sheet continues to move, the crushed area will increase, causing *V* and *H* to increase.

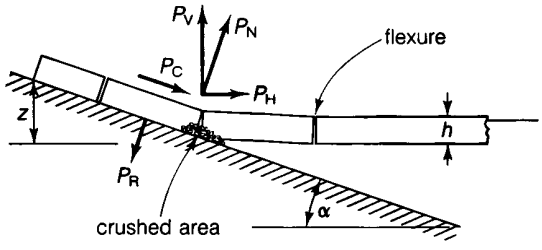

Fig H.1 Geometry for two-dimensional analysis of forces on a sloping

If the driving force is assumed to be unlimited, V and H will continue to increase until the ice fails. Except for very steep structures, the effect of H on the bending failure of the ice can be ignored. The ice sheet then behaves like a beam or plate on an elastic foundation. The load V to fail the ice sheet governs the initial lateral load on the structure. Subsequent loads are generally higher because of the additional load required to push the ice pieces up the slope. To appreciate the influence of various parameters it is useful to derive some simple equations using a two-dimensional system.

H.2.2 Derivation of two-dimensional analysis formula

Croasdale et al. (1978) proposed a two-dimension analysis model for ice interaction with a sloping structure. At the first contact between ice sheet and sloping structure, forces can derive the relationships between V, H, N and μ:

$$H = N\sin\alpha + \mu N\cos\alpha$$

$$V = N\cos\alpha - \mu N\sin\alpha$$

$$H = VC \qquad \text{(H-1)}$$

where $C = (\sin\alpha + \mu\cos\alpha)/(\cos\alpha - \mu\sin\alpha)$; α is the angle of the slope from the horizontal and μ is the friction coefficient.

When the moment capacity of the ice sheet is related to corresponding vertical force required to initiate failure, the horizontal force per unit width of the structure is given by

$$H / D = 0.68\,\sigma_f b\left(\rho_w g h^5 / E\right)^{0.25} C \qquad \text{(H-2)}$$

where D is the width of the structure, σ_f is the flexural strength of ice, $\rho_w g$ is the weight density of water, h is the ice thickness, and E is the elastic modulus of ice.
This gives the horizontal force generated at the instance of the first failure of the ice. Once the ice has failed, the broken pieces start to ride up the face of the structure, and an additional force is experienced by the structure. The corresponding total force experienced by the structure is

$$H / D = C_1\sigma_f\left(\rho_w g h^5 / E\right)^{0.25} + zh\rho_i g C_2 \qquad \text{(H-3)}$$

where $C_1 = 0.68C$, $C_2 = C(\sin\alpha + \mu\cos\alpha) + (\cos\alpha - \mu\sin\alpha)/\tan\alpha$, z is the maximum ride-up height, and $\rho_i g$ is the weight density of ice.

H.2.3 Factors affecting the failure modes.

Fig H.2 is the results of research from *Croasdale et al. (1980)* to show the relationship between failure mode and angles and friction. The strength affects the breaking component but not the ride-up component. In this simple two-dimensional elastic analysis, the ride-up force is typically larger than the breaking force, so the effect of ice strength on total force is not as significant. The effect of ice thickness is probably the most significant parameter affecting ice forces on sloping structure.

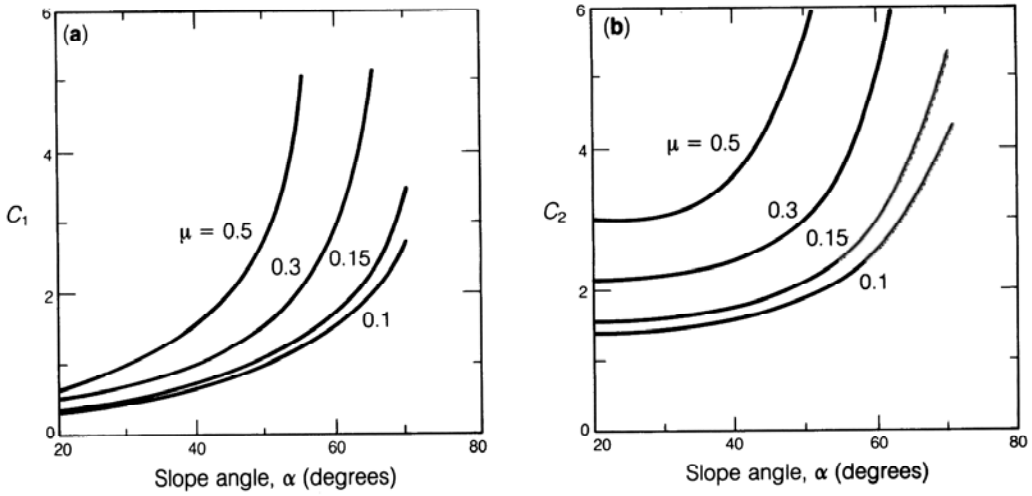

Fig-H.2 The coefficients C_1 and C_2 as a function of slope angle α and coefficient of friction μ (After *Croasdale, 1980*); (a) the coefficient C_1; (b) the coefficient C_2

H.2.4 Usage of two-dimensional analysis

The two-dimensional analysis is appropriate for very wide conical structure. For narrow structures, this is not a good approach, since the ice failure zone is much larger than the width of the structure.

H.3 Flexural failure

This approach is suitable for narrow sloping structures.

H.3.1 Empirical relationships

Edwards and *Croasdale (1976)* derived the empirical equation from a series of model tests on 45º cones with a friction coefficient of 0.05. The maximum horizontal force is

$$H = 1.6\sigma_f h^2 + 6.0\rho_w g D h^2 \qquad \text{(H-4)}$$

The first term represents the icebreaking component, while the second is the ice clearing component.

H.3.2 Elastic analysis

Nevel (1972) reduced the ice force problem to the prediction of the forces necessary to fail a series of ice wedges formed by radial cracking of the ice as it advances against a cone;

$$6P/b_0\sigma_f h^2 = 1.05 + 2.00(a/l) + 0.50(a/l)^3 \qquad \text{(H-5)}$$

where P is the failure force on the tip of the wedge, a is the distance from the tip of the wedge over which it is loaded, and b_0 is a constant. The characteristic length l for the plate is given by

$$l = \left[Eh^3/(12\rho_w g)\right]^{0.25} \qquad \text{(H-6)}$$

H.3.3 Plastic limit analysis

Ralston (1977) used three-dimensional plate theory, and plastic limit state analysis, where the work done by external forces is equated to the rate of energy dissipation. The

horizontal and vertical forces, respectively, exerted by ice failure in flexural can be determined by the equations:

$$H = A_4\left[A_1\sigma_f h^2 + A_2\rho_w g h D^2 + A_3\sigma_w g h\left(D^2 - D_T^2\right)\right] \quad \text{(H-7)}$$

$$V = B_1 H + B_2\rho_w g h_R\left(D^2 - D_T^2\right) \quad \text{(H-8)}$$

where A_1, A_2, A_3, A_4, B_1, and B_2 are the dimensionless coefficients, D is the waterline diameter of the cone, and D^T is the top diameter of the cone. The first term of equation H-7) is due to ice breaking, the second for buoyancy and the third for clearing.

Lau, Muggeridge and *Williams (1988)* presented the comparison of the same analysis with down ward breaking cone data. The load formulations of *H-7*) and *H-8*) have been developed for an upward breaking cone. For determining loads on down ward breaking cone, the same formulas and coefficients can be used, by replacing ρ_w by $\rho_w/9$ in the appropriate terms of above equations. The factor of 9 reflects the ratio between the forces to lift an ice floe out of the water, and to submerge it completely into the water.

Lau, Muggeridge and *Williams (1988)* also presented that there are some restrictions to using Ralston's equation. If the portion of the cone above the water level is too small, then the clearing forces may be underestimated. The Ralston's formulation may also not adequately predict loads on large-diameter caissons, or the loads associated with high velocity ice movements.

Frederking (1980)
Observations of ice behaviour on inclined plane structures of finite width reveal a typical cycle of ice-structure interaction to use a three-dimensional theory. This analysis is particularly appropriate for rectangular sloping caissons, rather than conical designs. For the case of low interaction speeds, the total horizontal force for breaking the ice (H_{br}), rotating it onto the surface (H_r), and sliding it up the incline (H_s) is given by

$$H_{br} = 0.33C\sigma_f h^2 \tan(\beta/2)\left[1.16 + 0.0325C + (2.26 + 0.0825C)a/l\right] \quad \text{(H-9)}$$

$$H_r = N_r \sin\alpha + \mu N_r \cos\alpha \quad \text{(H-10)}$$

$$H_s = N_s \sin\alpha + \mu N_s \cos\alpha \quad \text{(H-11)}$$

where $N_r = \bar{x}F_g/\left[l_b f(\phi)\right]$,

$\bar{x} = (l_b/6)\left[\left((3D/l_b) + 2\tan(\beta/2)\right)/\left((D/l_b) + \tan(\beta/2)\right)\right]$,

$F_g = \rho_i hA = \rho_i h l_b^2\left(D/l_b + \tan(\beta/2)\right)$,

$N_s = F_g \cos\alpha$,

$C = \left(\sin\alpha + \mu\cos\alpha\right)/\left(\cos\alpha - \mu\sin\alpha\right)$

in which σ_f is the flexural strength of ice, D is the width of the structure, β is the wedge angle, α is the truncation distance, l is the characteristic length, l_b is the breaking

distance, $1/f(\theta)$ is the static rotation force factor shown in graphical form by *Frederking*. For the maximum force which occurs at contact, $1/f(\theta) \simeq$ 1.8 for α =4.5º and 3.2 for α =60º.

H.4 Crushing failure

Michel (1978) has described the condition where ice sheets interact with inclined structures with angles to the horizontal of greater than 60º. For structures in this category, crushing failure will generally take place before flexure failure.

Danys and *Bercha (1975)* give the following formula for calculating horizontal and vertical ice forces on conical light piers.

$$H = mn_1 DH\sigma_c$$
$$V = mn_2 DH\sigma_c \qquad \text{(H-12)}$$

where m is the shape and contact coefficient, $n_1 = \cos^2\alpha$ and $n_2 = \cos\alpha \sin\alpha$, α is the slope with the vertical, D is the width of the structure at the water level, h is the effective ice thickness, and σ_c is the effective compressive strength of ice.

H.5 Adfreeze failure

Cammaert et al.(1984)

Ice adhering to offshore platforms may cause substantial horizontal forces on offshore platforms. The load required to fail and adfreeze bond on a conical structure can be much larger than the load associated with bending failure. Adfreeze problems may predominate in areas where ice may remain stationary for some time.

The load required to break the bond between the ice sheet and a conical structure over an angle 2θ is

$$H_a = C_a C_s Dh\tau_a I/\sin\alpha \qquad \text{(H-13)}$$

where C_a is an adfreeze factor to account for incomplete bonding (0.3 to 1.0), C_s is a stress factor to account for nonuniform stress distributions (0.7 to1.0), D is the structure diameter at the water line, and α is the cone angle to the horizontal. The value I is an elliptic integral which varies with α and θ, some representative values are shown below.

Failure zone angle (θ)	Cone angle				
	40°	50°	60°	70°	80°
75°	1.524	1.672	1.892	2.240	2.889
80°	1.612	1.760	1.981	2.329	2.987
85°	1.700	1.848	2.069	2.417	3.066
90°	1.787	1.936	2.157	2.505	3.152

H.6 References

[1] George D. Ashton, U.S Army Cold Regions Research and Engineering Laboratory, *River and Lake Ice Engineering* (1986), pp.125-146.

[2] A. W. Lipsett, *Field Measurements of Ice Forces on Bridge Piers* (1973-1979)

[3] K. Kato and D. S. Sodhi, *Ice Action on Pairs of Cylindrical and Conical Structure* (1983), CRREL Report 83-25.

[4] Mauri Määttänen, *On Conditions for the Rise of Self-excited Ice-induced Autonomous Oscillations in Slender Marine Pile Structures* (1978).

[5] Per Tryde, *Physics and Mechanics of Ice* (1980). IUTAM symposium Copenhagen 1979.

[6] T. Carstens, *Working Group on Ice Forces on Structures* (1980).

[7] Ken-ichi Hirayama, Joachim Schwarz, and Han-chin Wu, *An Investigation of Ice Forces on Vertical Structure* (1974).

[8] A. B. Cammaert and D. B. Muggeridge, *Ice Interaction with Offshore structures* (1988), pp.247-277.

[9] Stefan Karlsson and Peter Strindö, *Ice Forces on Cylindrical and Conical columns* (1985).

[10] Juri Kajaste-Rudnitski, Pauli Jumppanen, and William M. Sackinger, *Ice Loads upon a Cylindrical Offshore Structure* (1985).

[11] Austin Kovacs, *Estimating the Full-scale Tensile, Flexural and Compressive Strength of First-Year Ice*, CRREL Report 96-11(1996).

I SCHEMATIC MAP OF ICE CONDITIONS

I.1 Ice condition of the Arctic regions

The advantage of sloping and cone-shaped structures is that they induce bending failure. A general schematic map of ice conditions in the Arctic is shown in *Fig I.1*. The extent of ice cover is controlled by a complex combination of air conditions and sea conditions, but the influence of sea currents is particularly important. Each winter, most of the seas north of latitude about $60^{o}N$ are frozen. The ocean, especially the Norwegian Sea, is kept largely ice-free by the Gulf Stream. The east coast of Canada, on the other hand, experiences more southerly encroachment of first-year sea ice as a result of prevailing northerly winds and the cold Labrador Current from Greenland and the Arctic Islands.

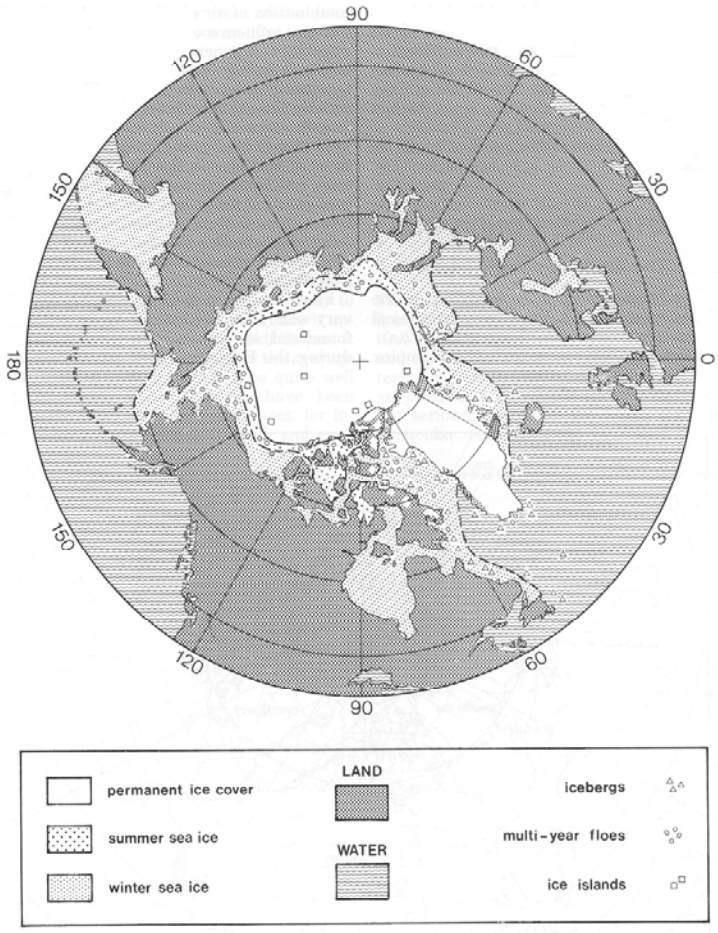

Fig I.1 Schematic map of Arctic ice conditions.

I.2 Ice condition in the Baltic

The Baltic Sea usually includes the whole area south and east of Sweden, including the Gulf of Bothnia, the Gulf of Finland, and the Gulf of Riga. The ice conditions in the Baltic are widely varied, and each sub-area constitutes a specific system with characteristic ice formation and disintegration processes. The northern part of the Gulf of Bothnia is entirely covered by sea ice four to five months per year and the southern part is not wholly covered and is more mobile. A characteristic of the Southern Baltic is that ice formation does not take place continuously; ice periods alternate with periods of no

ice. Hence, individual cold weather spells dictate ice formation and ice thickness. In the northern part of the Gulf of Riga, the eastern part of the Gulf of Finland, along the south coast of Finland and along all coasts of the Gulf of Finland and along all coasts of the Gulf of Bothnia, a belt of fast ice is formed every year. The Gulf of Bothnia is subjected to drifting winter first-year ice of thickness up to about 1 m, often rafted, with ridges up to 10 m thickness. However, ridges are seldom consolidated, and contains no multi-year ice or icebergs. The duration of the ice period increases from south to north; the longest ice period in the northern Gulf of Bothnia is from the middle of October until the end of June, almost approaching Arctic condition. The maximum ice thickness measured in the Baltic was 1.15 m, near Kemi in the 1941 to 1942 ice season. The mean ice thickness in this region is normally 0.75 m (*Palosuo, 1971*).

I.3 The maps of ice condition in the Baltic

The following figure obtained from SMHI (Swedish Meteorological and Hydrological Institute) is a routine chart for maximum ice extent in a severe winter (*1966. Feb. 22*,).

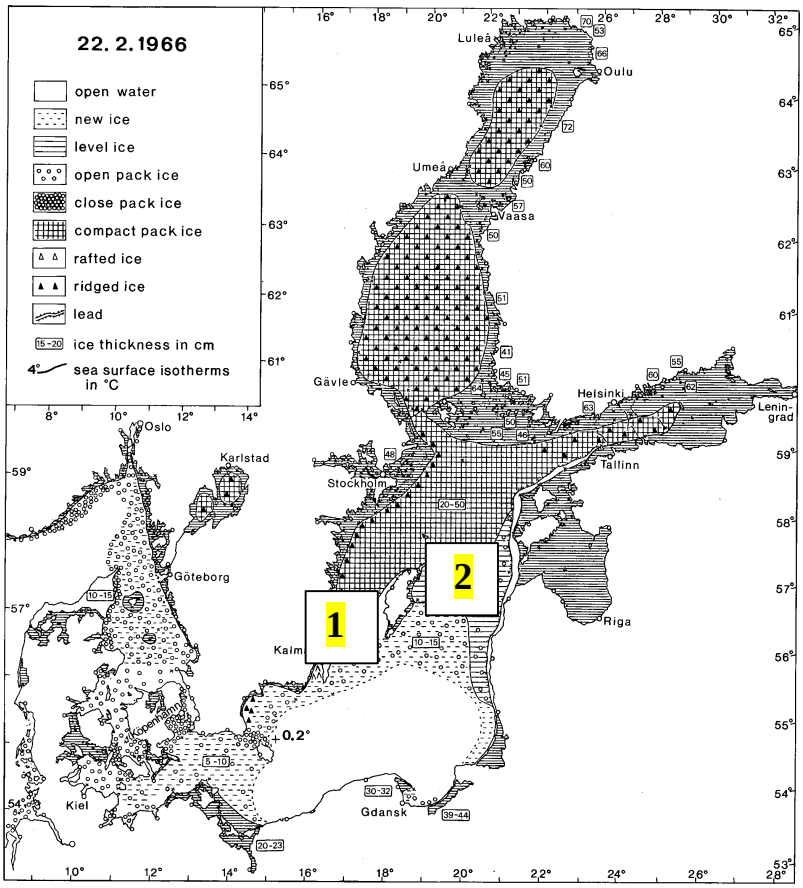

Fig I.2 the maximum ice extent in a severe winter *(1966. Feb.22,)*.

I.4 The ice thickness near Gotland of the Baltic

The ice thickness is shown in the following table (The probable places which the wind power plants would be installed). These data were obtained from SMHI, and is formed on data gathered during approximately 6months every year from 1963 to 1979.

Day	1	11	21	1	11	21	1	11	21	1	11	21	1	11	21	1	11	21	1	11	21	1
Month	11	11	11	12	12	12	1	1	1	2	2	2	3	3	3	4	4	4	5	5	5	6
Ice frequency	0	0	0	0	0	0	0	5	9	14	21	23	31	25	16	14	12	15	3	0	0	0
Thickness																						
1– 2 cm	0	0	0	0	0	0	0	0	0	0	0	0	9	0	0	0	0	0	0	0	0	0
3– 6 cm	0	0	0	0	0	0	0	0	50	29	23	0	41	19	0	0	0	0	0	0	0	0
7–12 cm	0	0	0	0	0	0	0	100	50	57	43	8	18	42	31	0	0	57	100	0	0	0
13–20 cm	0	0	0	0	0	0	0	0	0	0	27	38	0	0	31	25	60	43	0	0	0	0
21–30 cm	0	0	0	0	0	0	0	0	0	14	0	50	32	32	38	50	40	0	0	0	0	0
31–42 cm	0	0	0	0	0	0	0	0	0	0	0	0	0	6	0	17	0	0	0	0	0	0
43–56 cm	0	0	0	0	0	0	0	0	0	0	7	4	0	0	0	8	0	0	0	0	0	0
57–72 cm	0	0	0	0	0	0	0	0	0	0	0	0	0	0	0	0	0	0	0	0	0	0
>73 cm	0	0	0	0	0	0	0	0	0	0	0	0	0	0	0	0	0	0	0	0	0	0
Mean thickness	0	0	0	0	0	0	0	9	7	10	12	21	11	15	17	27	20	12	9	0	0	0
Number of ice years	0	0	0	0	0	0	0	1	1	3	3	3	6	6	5	1	1	2	1	0	0	0
Number of data	0	0	0	0	0	0	0	1	2	7	30	26	22	31	13	12	5	14	3	0	0	0

Table I.1 The ice thickness and frequency of western Baltic of Gotland island (NO.1)

Day	1	11	21	1	11	21	1	11	21	1	11	21	1	11	21	1	11	21	1	11	21	1
Month	11	11	11	12	12	12	1	1	1	2	2	2	3	3	3	4	4	4	5	5	5	6
Ice frequency	0	0	0	0	0	0	0	0	0	0	5	23	16	9	11	4	0	0	0	0	0	0
Thickness																						
1– 2 cm	0	0	0	0	0	0	0	0	0	0	0	0	0	0	0	0	0	0	0	0	0	0
3– 6 cm	0	0	0	0	0	0	0	0	0	0	0	10	11	0	20	0	0	0	0	0	0	0
7–12 cm	0	0	0	0	0	0	0	0	0	0	0	24	33	100	80	75	0	0	0	0	0	0
13–20 cm	0	0	0	0	0	0	0	0	0	0	100	52	56	0	0	25	0	0	0	0	0	0
21–30 cm	0	0	0	0	0	0	0	0	0	0	0	14	0	0	0	0	0	0	0	0	0	0
31–42 cm	0	0	0	0	0	0	0	0	0	0	0	0	0	0	0	0	0	0	0	0	0	0
43–56 cm	0	0	0	0	0	0	0	0	0	0	0	0	0	0	0	0	0	0	0	0	0	0
57–72 cm	0	0	0	0	0	0	0	0	0	0	0	0	0	0	0	0	0	0	0	0	0	0
>73 cm	0	0	0	0	0	0	0	0	0	0	0	0	0	0	0	0	0	0	0	0	0	0
Mean thickness	0	0	0	0	0	0	0	0	0	0	16	14	12	9	8	11	0	0	0	0	0	0
Number of ice years	0	0	0	0	0	0	0	0	0	0	1	3	2	1	1	1	0	0	0	0	0	0
Number of data	0	0	0	0	0	0	0	0	0	0	4	21	9	6	10	4	0	0	0	0	0	0

Table I.2 The ice thickness and frequency of eastern Baltic of Gotland island. (NO.2)

I.5 References

[1] Norbert Untersteiner, *The Geophysics of Sea Ice* (1986).

[2] G. A. Kuehn and E. M. Schulson, *The mechanical properties of saline ice under uniaxial compression*, (1994), pp.39-48.

[3] Kattegat, Skagerrak and Lake VäNERN, *Climatological Ice Atlas for the Baltic Sea,* (1963-1979).